A pipeline for validation of sRNA effectors suggests cross-kingdom communication in the symbiosis of *Arabidopsis* with *Serendipita indica*

Sabrine Nasfi[1], Saba Shahbazi[1], Katharina Bitterlich[1], Ena Šečić[1], Karl-Heinz Kogel[1,2]* & Jens Steinbrenner[1]

[1] Institute of Phytopathology, Research Centre for BioSystems, Land Use and Nutrition, Justus-Liebig-University Giessen, Heinrich-Buff-Ring 26, 35392 Giessen, Germany.

[2] Institut de biologie moléculaire des plantes, CNRS, Université de Strasbourg, 12 rue du Général Zimmer, 67084 Strasbourg, France

***Correspondence:**

karl-heinz.kogel@agrar.uni-giessen.de

All E-mail addresses:

Sabrine.Nasfi@agrar.uni-giessen.de (ORCID no.: 0000-0001-5916-0824)

Karl-Heinz.Kogel@agrar.uni-giessen.de (ORCID no.: 0000-0003-1226-003X)

Jens.Steinbrenner@gmail.com (ORCID no.: 0000-0003-1008-2268)

Ena.Secic@agrar.uni-giessen.de (ORCID no.: 0000-0002-6469-4895)

Shahbazi.saba@yahoo.com (ORCID no.: 0009-0005-9222-3715)

katha.bitterlich@gmail.com (ORCID no.: 0009-0003-5976-1322)

word count (including figure legends) ca. 7800; 10 figures; 8 Supplement figures

Highlight

Small RNAs of the beneficial fungus *Serendipita indica* are translocated and silence Arabidopsis genes at the onset of the interaction, revealing cross-kingdom communication in sebacinoid symbiosis.

Abstract

Bidirectional communication between pathogenic microbes and their plant hosts via small (s)RNA-mediated cross-kingdom RNA interference (ckRNAi) is one key element for successful host colonisation. However, whether mutualistic fungi from the Serendipitaceae family, known for their extremely broad host range, employ sRNAs to colonize plant roots is still under discussion. To address this question, we developed a pipeline to validate the accumulation, translocation, and activity of fungal sRNAs in post-transcriptional silencing of *Arabidopsis thaliana* genes. Using stem-loop PCR, we detected the expression of a specific set of *Serendipita indica* (*Si)*sRNAs, targeting host genes involved in cell wall organization, hormonal signalling regulation, immunity, and gene regulation. To confirm the gene silencing activity of these sRNA in plant cells, *Si*sRNAs were transiently expressed in protoplasts. Stem-loop PCR proved the expression of sRNAs, while qPCR validated post-transcriptional gene silencing of their predicted target genes. Furthermore, ARGONAUTE 1 immunoprecipitation (*At*AGO1-IP) revealed the loading of fungal *Si*sRNAs into the plant RNAi machinery, suggesting the translocation of *Si*sRNA from the fungus into root cells. In conclusion, this study provides a blueprint for rapid selection and analysis of sRNA effectors in plant-microbe interactions and further suggests cross-kingdom communication in the Sebacinoid symbiosis.

Keywords

Arabidopsis, AGO1-IP, cross-kingdom communication, *Serendipita indica,* sRNA, symbiosis, 5'-RLM-RACE, RNA interference

Abbreviations

AGO: argonaute

At: *Arabidopsis thaliana*

DCL: dicer-like

dpi: days post inoculation

hptr: hours post-transformation

IP: immunoprecipitation

miRNA: micro RNA

nt: nucleotide

PTGS: post-transcriptional gene silencing

RISC: RNA-induced silencing complex

RKN: root-knot nematodes

RNAi: RNA interference

Si: *Serendipita indica*

siRNA: small interfering RNA

sRNA: small RNA

Introduction

RNA interference (RNAi) is a regulatory process in most eukaryotes in which gene expression is silenced at the transcriptional or post-transcriptional level by the action of small (s) RNA; it is associated with the control of genome stability, developmental processes, and responses to biotic and abiotic stresses (Zhan and Meyers, 2023). Two types of sRNAs predominate in plants: micro (mi) RNAs are 20-22 nucleotides (nt) in length, processed from primary miRNAs (pri-miRNAs) containing a stem-loop structure encoded by microRNA (*MIR)* genes (Meyers and Axtell, 2019; Reinhart *et al.,* 2002). In contrast, small-interfering (si) RNAs are RNA molecules of 20-24 nt in length produced from longer endogenous RNA templates or from exogenous RNA sequences (viruses or transgenes). miRNA and siRNA precursors are processed by RNase III-like endonucleases named DICER-like (DCL), then bound by ARGONAUTE (AGO) proteins, which are incorporated into the RNA-Induced Silencing Complex (RISC), where they target complementary mRNA transcripts to induce post-transcriptional gene silencing (PTGS) (Iwakawa & Tomari, 2022). Plant sRNAs can also move intercellularly across plasmodesmata and systemically across the phloem, acting cell non-autonomously and can also translocate between interacting species (Zhan & Meyers, 2023). In the latter case, sRNAs are transferred bidirectionally between plant hosts and pathogenic microbes to modulate defence and virulence, a phenomenon called cross-kingdom RNAi (ckRNAi) (Göhre and Weiberg, 2023; Mahanty *et al*., 2023; Wang *et al*., 2017). ckRNAi in plant-pathogen interactions was discovered in 2013 when the necrotrophic fungus *Botrytis cinerea* was shown to induce silencing of host defence genes in *Solanum lycopersicum* and *Arabidopsis thaliana* (*At*) (Weiberg *et al.,* 2013). Since then, several reports supported the existence of ckRNAi (Wang & Dean, 2020) and showed that sRNA effectors exchange can be bidirectional (Zhang *et al.,* 2016; Cai *et al.,* 2018).

101 Already in 2006, Huang and colleagues reported reduced nematode infectivity
102 when root-knot nematodes (RKN) fed on roots of Arabidopsis plants expressing
103 double-stranded (ds) RNA targeting the *16D10* gene, which encodes a conserved
104 secreted RKN root growth-stimulating peptide known to be involved in parasitism
105 (Huang *et al.,* 2006). Later, it was shown that sRNA can indeed move from a plant
106 to an attacking pathogen in the interaction of barley and wheat with the powdery
107 mildew fungus (*Blumeria graminis*) (Nowara *et al.,* 2010). Transient transformation
108 with a plasmid overexpressing dsRNA directed against the fungal *AVR10* gene
109 increased the susceptibility of leaf epidermal cells to the corresponding *Blumeria*
110 *graminis* races, a technique termed host-induced-gene-silencing (HIGS). Since
111 then, numerous reports have shown that HIGS is an efficient strategy for pests
112 and disease control in crops (Cai et al., 2018; Koch et al., 2013; Liu et al., 2020; Sang
113 & Kim, 2020; Zand Karimi & Innes, 2022).

114 Although ckRNAi and related artificial processes such as HIGS were discovered in
115 plants more than 10 years ago, the molecular mechanisms are still not fully
116 understood. For instance, the mode of bidirectional transfer of RNAs in
117 extracellular vesicles (EVs) is still a matter of debate (He, Cai, *et al.,* 2021; He,
118 Hamby, *et al.,* 2021; Nasfi & Kogel, 2022; Rutter & Innes, 2018), and the occurrence
119 in mutualistic symbioses is little researched albeit a growing number of studies
120 are shedding light on ckRNAi in plant-symbiont interactions (Qiao *et al.,* 2023).

121 ckRNAi in mycorrhizal symbioses seems to include miRNA. For example,
122 Pmic_miR-8, a miRNA from the ectomycorrhizal fungus *Pisolithus microcarpus*
123 enhanced the colonization of its host *Eucalyptus grandis and* thus plays a role in
124 the beneficial ectomycorrhizal symbiosis (Wong-Bajracharya *et al.,* 2022). In
125 addition, recent *in silico* analysis of the sRNA population from *Rhizophagus*
126 *irregularis*, supported by degradome data from *Medicago truncatula*, has shown
127 that some sRNAs of Rhizophagus modulate root colonization (Silvestri *et al.,* 2019).
128 Moreover, tRFs identified in root nodule symbioses between soybean and the

129 bacterial symbiont *Bradyrhizobium japonicum* hijack *Glycine max* AGO1 and are
130 positive regulators of rhizobial infection and nodule formation (Ren *et al.,* 2019),
131 further emphasising the existence of ckRNAi in plant-mutual interactions.

132 Key to understanding ckRNAi is the identification and functional validation of
133 translocated sRNA (sRNA effectors), and tools are needed to study the mode of
134 action of numerous sRNAs derived from extensive sRNA sequencing data. Here,
135 we report on a pipeline for sRNA effectors validation by studying the interaction
136 between the mutualistic basidiomycete fungus *Serendipita indica* (*Si*) and the dicot
137 model plant *Arabidopsis thaliana* (*At*). The fungus was originally isolated from the
138 roots of the shrubs *Prosopis juliflora* and *Ziziphus nummularia* in the Indian Thar
139 desert (Verma *et al.,* 1998). Its beneficial activity includes plant growth promotion,
140 plant resistance priming, enhanced nitrate and phosphate delivery, promotion of
141 adventitious root and root hair formation, early flowering, support of higher seed
142 yield, alteration in secondary metabolites, and hardening of tissue cultured plants
143 (Glaeser *et al.,* 2016; Qiang *et al.,* 2012; N. Verma *et al.,* 2022; Weiß *et al.,* 2016; Xu
144 *et al.,* 2018; Zuccaro *et al.,* 2011). The fungus transfers protein effectors to host
145 cells to exploit the host´s metabolism and promote microbial colonization (Akum
146 *et al.,* 2015; Osborne *et al.,* 2023). To further explore the molecular basis of the
147 mutualistic interaction formed by *Si* with a wide range of plants (Sebacinalean
148 symbiosis), we recently demonstrated the global change in sRNA profiles in the
149 interaction of the fungus and the grass model *Brachypodium distachyon* (*Bd*) (Šečić
150 et al., 2021). Among *Bd*- and *Si*-generated sRNAs with putative functions in the
151 interacting organism, we found proteins involved in cell wall organization,
152 hormonal signalling regulation and immunity as potential targets of putative
153 fungal sRNA effectors.

154 Building upon the findings from our prior work (Šečić et al., 2021), we have
155 selected a set of fungal sRNAs with interesting predicted *At* targets to further
156 investigate their activity in the *Si-At* interaction. We developed a functional

157 protoplast assay to validate potential putative fungal sRNA effectors assessing
158 their gene-silencing activity. Using stem-loop PCR, we confirmed sRNA
159 transformation and expression in plant protoplasts and recorded the
160 downregulation of predicted host target genes via qPCR. Additionally, we
161 investigated the capability of *Si*sRNA effector candidates in mediating the
162 degradation of host mRNA by 5'-RLM-RACE. Finally, *At*AGO1 immunoprecipitation
163 assay, confirmed the loading of fungal *Si*sRNAs into the plant's RNAi machinery.
164 The data support the existence of naturally occurring ckRNAi between the
165 mutualistic fungus *Serendipita indica* and *Arabidopsis thaliana*.

166

167 **Materials and methods**

168 **Plant material and growth conditions**

169 For protoplast isolation, *Arabidopsis thaliana* plants of ecotype Columbia-0 (Col-0)
170 were cultivated in a 4:1 ratio of T-type soil (F.-E. Typ Nullerde, Hawita) and crystal
171 quartz sand mixture for 4 to 5 weeks in a growth chamber in a 19°C day/18°C night
172 (9 h of light, 150 µmol photons m^{-2} s^{-1}) and a constant relative humidity of 60%. For
173 interaction studies of *At* roots and *Serendipita indica* (IPAZ-11827, Institute of
174 Phytopathology, Giessen, Germany), plants were grown on vertical square Petri
175 dishes on an ATS medium (Lincoln *et al.,* 1990) without sucrose and supplemented
176 with 4.5 g/L Gelrite (Duchefa #G1101) in a 22°C day/18°C night cycle (8 h of light).
177 Roots of 14-day-old plants were inoculated with 1 mL of a suspension of 500,000
178 chlamydospores/mL in aqueous 0.02% Tween 20 per Petri dish.

179

180 **sRNA sequencing and Arabidopsis target prediction**

181 In our previous study (Šečić *et al.,* 2021) we investigated changes in mRNA and
182 sRNA expression profiles during the mutualistic interaction between *Serendipita*
183 *indica* and the grass model *Brachypodium distachyon* using high throughput

184 sRNAseq and transcriptome analysis. Raw sRNA sequencing data underwent
185 bioinformatic filtering steps, as detailed in Šečić *et al* 2021, and were aligned to the
186 genomes and transcriptomes of both organisms. *Si*sRNAs were categorized into
187 two groups: endogenous *Si*sRNAs present in axenic fungal culture, and putative
188 ck-*Si*sRNAs exhibiting higher abundance in the colonized *Bd* roots, therefore
189 potentially playing a crucial role in the establishment of RNAi mediated mutualism.
190 Size distribution analysis of the putative ck-*Si*sRNAs revealed a prominent peak of
191 21 nt molecules in the *Si-Bd* samples. By focusing on 21 nt *Si*sRNAs, we identified
192 412 unique induced putative ck-sRNAs, of which carry 30% adenine (A), 26% uracil
193 (U), 21% cytosine (C) and 22% guanine (G) at their 5´-end.

194

195 **Plasmid construct**

196 *At*MIR390a distal stem-loop was digested from the pMDC32B-*At*MIR390a-B/c
197 vector (Plasmid #51776, https://www.addgene.org, Carbonell *et al.,* 2014) using
198 Fast digest enzymes EcoRI and HindIII (Thermo Fisher Scientific, FD0274 &
199 FD0505). The pUC18-*At*MIR390a-B/c construct was generated by ligating the
200 *At*MIR390a precursor into the pUC18 vector (plasmid #50004) backbone using T4
201 DNA Ligase (Thermo Fischer Scientific, EL0011). The *RFP* insert was digested from
202 the pBeaconRFP_GR vector (https://gatewayvectors.vib.be/index.php/ ID: 3_20,
203 Bargmann & Birnbaum, 2009) using the restriction enzyme NdeI (NEB, R0111S)
204 and further ligated into the NdeI site of the pUC18-*At*MIR390a-B/c vector. 75mer
205 oligonucleotides comprising the amiRNAs and *Si*sRNAs sequences were cloned
206 into the BsaI-sites by Golden Gate strategy using BsaI-HF®v2 (NEB, R3733) and T4
207 DNA Ligase (Thermo Fischer Scientific, EL0011) in a single reaction, replacing the
208 toxic ccdB gene which allows the selection of 75-mer-positive clones. Before
209 cloning 75-mer oligonucleotides, a third BsaI-site in the pUC18 backbone which
210 would interfere with the Golden-Gate cloning was removed by site-directed
211 mutagenesis using Phusion High-Fidelity DNA polymerase (Thermo Fisher

212 Scientific, F553S) and the Fast digest Dpn I endonuclease (Thermo Fisher Scientific,
213 FD1703) as well as custom-designed site-directed mutagenesis primers pUC18-
214 Mut-Fwd and pUC18-Mut-Rev.
215 The artificially designed amiRNAs, their 5´- nucleotide, their predicted targets,
216 their target aligned fragment, and their expectation value are listed in
217 Supplemental Tables 1. Same details of the selected putative ck-*Si*sRNAs cloned in
218 the expression vector for further PTGS analysis are listed in Supplemental Table 2.
219 Supplemental Figure 1 illustrate an alignment between amiRNAs and *Si*sRNA and
220 their predicted selected targets as displayed by psRNATarget web-tool. 75-mer
221 oligonucleotides for amiRNAs and *Si*sRNAs were designed following the P-SAMS
222 algorithm developed by the James Carrington lab (Fahlgren *et al.,* 2016) available
223 at http://p-sams.carringtonlab.org. 75 mer oligonucleotides of amiRNAs and
224 *Si*sRNAs are listed in Supplemental Table 3. An *in-silico* cloning design was
225 performed using Snapgene software (www.snapgene.com) and the final pUC18-
226 *At*MIR390a-RFP-sRNA vector map is shown in Supplement Figure 2.
227
228 **Protoplast transformation**
229 The "Tape-Arabidopsis Sandwich" method was used for protoplast isolation (Wu
230 *et al.,* 2009). The transformation was performed following the transient expression
231 of recombinant genes using the Arabidopsis mesophyll protoplast (TEAMP)
232 approach (Yoo *et al.,* 2007) with minor modifications. Since the transformation of
233 protoplasts was key to all subsequent experiments, we attempted to optimize its
234 efficiency by varying *i.* protoplast concentration (10x 10^4 and 5x 10^4
235 protoplasts/mL), *ii.* plasmid concentration (20 µg, 30 µg, and 40 µg) pUC18-
236 *At*MIR390a-RFP-sRNA and *iii*. incubation time (24 and 48 h). High transformation
237 efficiency was reported when using 5x 10^4 protoplasts/ml with a plasmid
238 concentration of 30 µg and an incubation time of 24 h, which was comparable to
239 the reported transformation efficiencies of *At* leaf protoplasts (Yoo *et al.,* 2007).
240 Total cell numbers were counted using a Fuchs-Rosenthal counting chamber

241 under an optical microscope. A microscopic check of protoplast transformation
242 was done using an epifluorescence microscope (TCS SP2 Leica). Images were
243 acquired with the image software Leica Application Suite (LAS) and all counting
244 was performed in triplicates. Transformed protoplasts were stored at -80°C for
245 further studies.
246
247 **RNA extraction and quality analysis**
248 Total RNA was extracted from protoplasts using QuickRNA™ Miniprep Kit (Zymo
249 Research, R1050) with an on-column DNase I treatment. Total RNA from *Si-At*
250 interaction growing on ATS plates was extracted using Direct-zol RNA Miniprep
251 (Zymo Research, R2051) with an on-column DNase I treatment. The RNA
252 concentration was determined with the NanoDrop ND-1000 Spectrophotometer
253 (Thermo Fisher Scientific, USA) and the purity was determined by measuring
254 A260/280 and A260/230 ratios. The quality of the RNA extracted from transformed
255 protoplasts was checked using the Agilent 2100 Bioanalyzer Nano Chip (Agilent,
256 Germany).
257
258 **Stem-Loop PCR**
259 Designed amiRNAs and *Si*sRNAs sequences were used as templates to design
260 specific stem-loop (SL) primers matching the corresponding sRNA over six nt at
261 the 3´end. Hairpin primers (cDNAhp) and forward primers were designed using
262 the tool published in Adhikari et al (2013) based on Varkonyi-Gasic et al., (2007)
263 (Adhikari *et al.,* 2013; Varkonyi-Gasic & Hellens, 2011). Stem-loop PCR was
264 performed as described (Werner *et al.,* 2021). End-point PCR was used to assess
265 the expression of amiRNAs and *Si*sRNAs. The PCR program was optimized to 95 °C
266 for 5 min; followed by 40 cycles of 95 C for 30 s, 60°C for 30 s, 72°C for 30 s; and
267 72°C for 5 min and then held at 4°C. PCR products were separated and visualized
268 in 2% TBE-agarose gels. Stem-loop PCR primers are listed in Supplemental Table
269 4.

270

271 **PTGS detection by qPCR**

272 The standard curve method was used to test the efficiency of the qPCR transcript
273 primers using a serial dilution of *At* cDNA library along with 3 different primer
274 concentrations (0.4 µM, 0.2 µM and 0.1 µM for each primer) and 5 µL of SybrGreen
275 (Sigma-Aldrich). The total volume of 10 µL and three technical replicates are
276 considered for each reaction. Before master mix preparation, 2 µL ROX (CRX
277 reference dye, Promega, C5411) were added to 1 mL SybrGreen as a passive
278 reference dye that allows fluorescent normalization for qPCR data. For the
279 preparation of cDNA first strands, 500 ng of RNA samples from transformed *At*
280 protoplasts and control protoplasts were used. qPCR was performed using the
281 QuantStudio 5 Real-Time PCR system (Applied Biosystems) in the 384-well plate as
282 follows: 50°C for 2 min, 95°C for 10 min, followed by 40 cycles of 95°C for 15 s, and
283 60°C for 1 min, with an additional melt curve stage consisting of 15 s at 95°C, 1
284 min at 60°C, and 15 s at 95°C.

285 To evaluate the relative quantification of *At* transcripts by qPCR, the gene
286 expression level was standardized to the control protoplasts. Fold change of *ΔΔ*ct
287 values and standard errors were calculated for all mean values. All qPCR primers
288 are listed in Supplemental Table 5.

289

290 **5´-RLM-RACE**

291 RNA ligase-mediated rapid amplification of cDNA ends (5´-RLM-RACE) was
292 performed using FirstChoice® RLM-RACE kit (Thermo Fisher Scientific) following
293 the manufacturer protocol and omitting the dephosphorylation and decapping
294 steps. One µg of RNA isolated from *At* protoplasts and control protoplasts were
295 used as a template and ligated to the 5´-RACE adapter using T4 RNA Ligase [10
296 U/µL] (Thermo Fisher Scientific). The ligation reaction was used entirely to
297 generate the first cDNA strand. Two rounds of nested hot-start touch-down PCR
298 were performed using outer (first) and inner (second) 5´-RLM-RACE universal

299 primers in combination consecutively with gene outer specific and gene inner
300 specific primers. PCR products were evaluated in a 1.5% agarose gel and bands of
301 the expected size were excised. Products were cleaned with the Wizard® SV Gel
302 and PCR Clean-Up System (Promega) and cloned with the pGEM®-T Vector Systems
303 (Promega). For each band, six clones were selected for sequencing at LGC
304 genomics. The oligonucleotides used are listed in the Supplemental Table 6.
305

306 **T-vector cloning and sequencing**

307 Stem-loop PCR and 5´-RLM-RACE PCR amplification products were purified using
308 The Wizard® SV Gel and PCR Clean-Up System (Promega). Cloning of the different
309 PCR products was performed as described in the pGEM®-T Vector system
310 according to the instructor´s instructions (Promega). Sequencing was performed
311 at LGC Genomics (Berlin, Germany) and analysed using the Snapgene tool (GSL
312 Biotech, available at snapgene.com). All PCR primers are presented in
313 Supplemental Table 7.
314

315 **AGO-IP**

316 *At*AGO1-Co-immunoprecipitation (Co-IP) was performed as described in the
317 publication of Dunker et *al.,* 2021 with modifications. Five gram of *Si* mycelium or
318 *At* roots inoculated or uninoculated with *Si* were ground to a fine powder using a
319 precooled mortar and pestle. To each sample, 20 mL of immunoprecipitation
320 extraction buffer was added, and samples were centrifuged at 3,200x g for 15 min
321 at 4°C to remove root debris. The supernatants were filtered through double-
322 layered Miracloth and 200 µL crude extract (CE= supernatant before antibodies)
323 was collected and combined with 50 µL 5X protein SDS loading buffer for western
324 blot analysis. 5 µL of anti-AGO1 polyclonal antibody (Agrisera, Catalog number:
325 AS09527) and 200 µL of protein A agarose beads (Roche, Ref: 11719408001) were
326 added to the remaining supernatant and incubated for 2 h at 4°C on a rotation
327 wheel. The samples were centrifuged at 200x g for 30 sec at 4°C. From the

328 supernatants, 200 µL were removed (SN after antibodies) and 50 µL of 5x protein
329 SDS loading buffer was added for further western blot analysis. The remaining
330 supernatants were discarded, and 1 mL of ice-cold IP wash buffer was added to
331 the pelleted beads and centrifuged at 200x g for 30 sec at 4°C. The pellet beads
332 were washed 3 times and finally resuspended in 1 mL wash buffer. Resuspended
333 pellet beads were divided into 30% for further WB analysis supplemented with 1x
334 protein SDS loading buffer (IP fraction) and 70% was used for sRNA recovery.

335 **sRNA recovery from IP fraction**

336 IP fractions were pelleted and 300 µL IP wash buffer was added together with 150
337 µL RNA release buffer. Samples were incubated in a thermoshaker for 15 min at
338 300 rpm at 65°C. 450 µL of water-saturated phenol was added and samples were
339 vortexed for 2 min then centrifuged at 10,000x g at room temperature (RT) for 8
340 min. The upper aqueous phase containing the sRNAs was transferred into a low-
341 binding RNA tube. 450 µl of chloroform/isoamyl alcohol (24:1) (Carl Roth,
342 Germany) was added to the RNA samples. The step was repeated twice. For RNA
343 precipitation, 0.1x volume of 3 M sodium acetate, 2.5x volume of 96% ethanol, and
344 20 µg RNA grade glycogen (Thermo Fisher Scientific, R0551) were added to the
345 RNA samples and placed overnight at -20°C. Samples were pelleted at 20,000x g
346 for 30 min at 4°C and pellets were washed with 500 µL 80% ethanol. RNA was
347 pelleted at 20,000x g for 20 min at 4°C, ethanol was removed, and pellets were air
348 dried until ethanol was completely evaporated. The RNA pellets were resuspended
349 in 8 µL DEPC-treated water and stored at -80°C.

350

351 **Western Blot analysis**

352 For western blot analysis, a 5.5% stacking gel and a 12% resolving gel were used.
353 For each sample, 20 µL of crude extract before antibodies (CE), supernatant after
354 pelleting agarose beads (SN), and *At*AGO1 co-IP fraction (IP) were loaded. All
355 samples were boiled at 95°C for 5 min before loading. Gel separation was
356 conducted at 100 V until the SDS loading buffer reached the edge of the gel

357 (electrophoresis takes approximately 2.5 h to 3 h). For immunodetection, a PVDF
358 blotting membrane (Carl Roth, Germany) was used. The blot was prepared in a
359 sandwich method in the following order: 4x Whatman paper (GE Healthcare, USA),
360 PVDF membrane, SDS-Gel, and 4x Whatman paper. Whatman papers were soaked
361 in Towbin buffer and the membrane was activated in methanol and washed with
362 Towbin buffer before transfer for equilibration. Blotting was performed using
363 BioRad TransBlot Turbo at 25 Volt and 1.0 Ampere for 30 min. The Blotting
364 sandwich was disassembled, and the membrane was washed with 1x PBS-T (0.1%
365 Tween) and then blocked for 1 h at RT with 10 mL 1x PBS-T (0.1% Tween) and 5%
366 (w/v) milk powder (CarlRoth, Germany). For detection of *At*AGO1 protein, the
367 membrane was incubated overnight at 4°C on a shaker with primary antibody
368 solution 1 µg/µL diluted 1:4000 anti-AGO1 (Agrisera, AS09 527) in 10 mL 1% milk
369 in 1x PBS-T. The membrane was washed 4 times for 10 min on a shaker at RT with
370 1x PBS-T and incubated for 2 h at RT with the secondary antibody IRDye® 800CW
371 Goat anti-Rabbit IgG (LI-COR, 926-32211) in 10 mL 1% milk in 1x PBS-T. The
372 membrane was washed 4 times for 10 min on a shaker at RT with 1x PBS-T. For
373 the membrane development, chemiluminescent substrates were applied
374 according to the manufacturer's recommendation, and images were captured
375 using the Bio-rad ChemiDoc MP imaging system.
376
377 **Statistical Analysis**
378 To assess the downregulation of *At* genes via qPCR, the 2−ΔΔCt method (Livak &
379 Schmittgen, 2001) was used for the quantification of *At* target transcript. The
380 results are expressed as values of the fold change of the transcript expression
381 level in comparison to the control and compared using a two-sided unpaired
382 student *t* test. Data showed a normal distribution in the Shapiro-Wilk test or
383 D´Agostino & Pearson test.
384

385 **Results**

386 We developed a pipeline for the validation of sRNA gene silencing activities in the
387 mutualistic interaction of *Serendipita indica* and *Arabidopsis thaliana*, comprising i.
388 prediction of *Si*sRNA Arabidopsis target genes, ii. validation of the gene silencing
389 activity of *Si*sRNAs in *At* protoplasts, iii. detection of fungal sRNAs (*Si*sRNAs) in
390 axenic culture and *Si*-colonized roots, and iv. detection of the association of
391 *Si*sRNAs with the *At*AGO1 protein (Figure 1).

392 ***Si*sRNA selection and Prediction of Arabidopsis targets**

393 Considering the broad host range of *Si*, we selected 14 induced ck-*Si*sRNAs from *Si*
394 non-coding regions based on their expression levels in colonized *Bd* roots and we
395 predicted their targets in *At* using psRNAtarget Scheme 2 (2017) default (Dai et al.,
396 2018). Among the predicted targets, we prioritized those with intriguing
397 descriptions and where a single *Si*sRNA has multiple target genes. Supplemental
398 Table 8 illustrates a summary of the 14 selected putative ck-*Si*sRNA, their raw read
399 counts normalized to *Si*-colonized *Bd* roots or to *Si* axenic, their 5´- nucleotide, and
400 their induction level. Supplementary File 2 illustrates *At* predicted targets for the
401 14 selected ck-*Si*sRNAs.

402

403 **amiRNAs mediate PTGS in transformed Arabidopsis protoplasts**

404 Arabidopsis protoplasts are a reproducible and cost-effective model system to
405 validate the expression and the potential silencing activity of *Si*sRNA on predicted
406 *At* target genes. To confirm the reliability of the system, we first used artificial
407 microRNAs (amiRNAs). The use of amiRNAs allowed the amiRNA-mRNA binding to
408 be manipulated, as they are artificially designed to have almost complete
409 complementarity with the mRNA target gene, unlike naturally occurring *Si*sRNAs,
410 which have varying degrees of mismatch with their predicted target genes. To this
411 end, we designed four amiRNAs of 21 nt (amir21, amir24, amir154, and amir296)
412 that almost fully match their predicted target genes (*AT5G25350*, *AT2G39020*,

413 *AT4G32160,* and *AT2G45240*, respectively) and exhibit a U at their 5´-end.
414 Subsequently, the four amiRNAs were cloned into the pUC18-*At*MIR390a-RFP
415 vector and transformed into *At* protoplasts, reaching a transformation efficiency
416 of 65% to 90% (calculated as the ratio between the red fluorescing protoplasts and
417 the total number of viable protoplasts; Supplemental Figure 3). The four amiRNAs
418 were successfully expressed in protoplast as detected by duplexed stem-loop PCR
419 (Figure 2). Amplification products were cloned into the pGEM-T® cloning vector
420 and sequencing confirmed amiRNAs sequences.

421 Supplemental Table 2 provides information on these amiRNAs, including their 5'-
422 terminal nucleotides, their predicted *At* target genes, their target aligned fragment,
423 and their target prediction expectation values, indicating the degree of
424 mismatches between the amiRNAs and the *At* target sequence, Supplemental
425 Table 9 provides a description and the expression level of the predicted *At* target
426 genes in leaf and root (Data extracted from Moreno et al., 2022).

427 Analysis of amir target downregulation was quantified by qPCR 24 h after the
428 transformation of amiRNAs into protoplasts and was 68% for *AT5G25350*, 43% for
429 *AT2G39020*, 50% for *AT4G32160*, and 65% for *AT2G4524*0, respectively (Figure 3).

430

431 **5'-RLM-RACE reveals canonical cleavage in protoplasts transformed with**
432 **amiRNA**

433 We selected amir296 and its predicted target gene *AT2G45240* to investigate the
434 canonical PTGS cleavage site using RNA-ligase-mediated Rapid Amplification of
435 cDNA Ends (5'-RLM-RACE) (Llave *et al.,* 2002; Ueno *et al.,* 2022). Samples were
436 obtained from transformed protoplasts at 24 hptr, from control protoplasts
437 (mock-treated without amiRNA construct) and from non-treated protoplasts. A
438 distinct band of approximately 383 bp was amplified from protoplasts expressing
439 amir296, consistent with the expected size of the canonical cleavage product

440 predicted to be targeted by amir296. Unexpectedly, weaker DNA fragments of a
441 similar size were detected in both control and non-treated protoplasts (Figure 4A).
442 Cloning and subsequent sequencing of the amplicons confirmed that all
443 sequences aligned with the *AT2G45240* sequence, and 50% of the obtained
444 sequences from protoplasts transformed with pUC18-*At*MIR390a-RFP-amir296
445 (three of six clones) exhibited the canonical cleavage site between nucleotide 10
446 and 11 of amir296. In contrast, PCR products from control and non-treated
447 protoplasts contained an *AT2G45240* fragment but did not correspond to a
448 canonical cleavage site, suggesting a possible cleavage by an endogenous miRNA
449 near the amir296 binding site or an RNA degradation (Figure 4B).

450

451 **Predicted *Si*sRNAs effectors are present in axenic cultures of *Serendipita***
452 ***indica***

453 After validation of the protoplast transformation strategy with artificial
454 microRNAs, we next wanted to further characterize in the same system putative
455 ck-*Si*sRNAs that we detected in our previous study in the *Si-Bd* symbiosis (Šečić *et*
456 *al*., 2021). From the data set of 412 putative fungal ck-RNAs, we selected a set of
457 14 *Si*sRNA of 21 nt on the basis that they showed a higher expression level in
458 colonized *Bd* roots, covered all four 5'-terminal nucleotides, and had interesting
459 Arabidopsis predicted targets, involved in cell wall organisation, regulation of
460 hormone signalling, immunity, and gene regulation. Using multiplexed stem-loop
461 PCR followed by gel electrophoresis, we detected all 14 *Si*sRNAs in 4-week-old
462 axenic *Si* culture (Figure 5). Next, we cloned a random subset of 6 out of 14 *Si*sRNAs
463 (*Si*sRNA21, *Si*sRNA2*3*, *Si*sRNA24, *Si*sRNA28, *Si*sRNA154, and *Si*sRNA296) and
464 subjected them to Sanger sequencing, which further confirmed the expected
465 *Si*sRNA sequences.

466

467 **Predicted *Si*sRNAs effectors are present in colonized *Arabidopsis thaliana***
468 **roots**

469 Next, we analysed the presence of a random subset of *Si*sRNAs (*Si*sRNA21,
470 *Si*sRNA23, *Si*sRNA24, *Si*sRNA25, *Si*sRNA26, *Si*sRNA28, *Si*sRNA37, *Si*sRNA47, and
471 *Si*sRNA62) (Supplemental Table 8) in *Si*-colonized *At* roots. Roots of 14-day-old
472 seedlings were inoculated with chlamydospores and harvested at 3-, 7-, and 14
473 days post-inoculation (dpi). Fungal colonization of roots was confirmed after 7
474 days both by confocal laser scanning microscopy (CLSM) using the chitin-specific
475 dye Wheat Germ Agglutinin with Alexa Fluor 488 (WGA-AF-488) (Figure 6 A) and by
476 PCR using Internal Transcribed Spacer (Si*ITS)* primers and *Si*-specific *Ubiquitin*
477 primers (Supplemental Figure 4). Multiplexed stem-loop PCR of total RNA
478 extracted from *Si*-colonized *At* roots at different time points detected eight out of
479 nine *Si*sRNAs (Figure 6 B). Bands for *Si*sRNA21 and *Si*sRNA24 did not consistently
480 show up at all three-time points, likely because of the limitations associated with
481 multiplexing the hairpin cDNA primers (Colombo *et al.,* 2013; Kramer, 2011;
482 Varkonyi-Gasic and Hellens, 2011). Consistent with this notion, the expression of
483 *Si*sRNA21 and *Si*sRNA24 was detected at 7 dpi using stem-loop PCR with less
484 multiplexing (Supplemental Figure 5). A random subset of the detected *Si*sRNAs
485 (*Si*sRNA21, *Si*sRNA24, *Si*sRNA28, *Si*sRNA154) were cloned and submitted for Sanger
486 sequencing, confirming the expected *Si*sRNA sequences in *Si*-colonized *At* roots.

487

488 **Predicted *Si*sRNAs effectors mediate PTGS in transformed Arabidopsis**
489 **protoplasts**

490 Next, we transiently transformed protoplasts with *Si*sRNAs to demonstrate their
491 gene-silencing activity. *At* protoplasts were transformed with a *35S::AtMIR390a*
492 expression construct containing *Si*sRNA21, *Si*sRNA24, *Si*sRNA28 and *Si*sRNA154,
493 respectively, (confirmed in *Si* axenic culture). Duplexed stem-loop PCR confirmed
494 the expression and amplification of the four *Si*sRNAs. (Figure 7). The amplification

495 products were cloned into the pGEM-T® cloning vector and sequencing confirmed
496 their identity.

497

498 Next, we investigated the ability of the expressed *Si*sRNAs to induce PTGS of
499 predicted target genes in protoplasts. *Si*sRNA24 was predicted to target five *At*
500 genes: *AT1G57590 (PECTIN ACETYESTERASE 2)* involved in cell wall organization,
501 *AT1G63180 (UDP-D-GALACTOSE 4-EPIMERASE 3)* involved in pollen development,
502 *AT1G65090 (SEED LIPID DROPLET PROTEIN1*) involved in lipid droplet-plasma
503 membrane tethering, *AT4G15765 (FAD/NAD(P)-binding oxidoreductase family*
504 *protein)* involved in jasmonic acid-mediated signalling, and *AT5G16680* (PAIPP2,
505 PHD2) involved in regulation of gene expression (see Supplemental File 2 and
506 Supplemental Table 9). Expression of *Si*sRNA24, which has U at the 5'-terminus,
507 and thus a preference for AGO1 (Mi *et al.*, 2008; Montgomery *et al.*, 2008; Takeda
508 *et al.*, 2008), significantly reduced the mRNA abundance of *AT1G63180*, *AT1G65090*,
509 *AT4G15765* and *AT5G16680* in protoplasts 24 h after transformation by 63%, 56%,
510 45%, and 73%, respectively, (Figure 8 B). Similarly, *Si*sRNA154, also with 5´ U, is
511 predicted to target *AT2G47600 (MAGNESIUM/PROTON EXCHANGER)* involved in
512 magnesium, iron and zinc ion transport and *AT4G32160 (Phox (PX) domain-*
513 *containing protein)* involved in signal transduction and previously investigated for
514 PTGS in protoplasts transformed with amir154. Expression of *Si*sRNA154
515 significantly downregulated the accumulation of *AT2G47600* mRNA by 37% but not
516 of *AT4G32160* (Figure 8 D). *Si*sRNA28 has 5' Adenine (A), therefore a loading
517 preference for AGO2 and AGO4 (Mi et al., 2008; Montgomery et al., 2008; Takeda
518 et al., 2008). Expression of *Si*sRNA28 in protoplasts did not result in
519 downregulation of any of the three predicted target genes: *AT1G05180 (AUXIN*
520 *RESISTANT 1*) involved in auxin-activated signalling pathway and response to
521 cytokinin, *AT5G55930* (*ARABIDOPSIS THALIANA OLIGOPEPTIDE TRANSPORTER 1*) an
522 oligopeptide transporter, and *AT3G06670* (*PLATINUM SENSITIVE 2 LIKE*) with a

523 regulatory function in ncRNA processing (Figure 8 C). Finally, expression of
524 *Si*sRNA21 with 5' Cytosine (C) and thus a preference for AGO5 (Mi et al., 2008;
525 Montgomery et al., 2008; Takeda et al., 2008) resulted in downregulation of
526 predicted target transcripts *AT5G25350* (a negative regulator of the ethylene-
527 activated signalling pathway and previously investigated for PTGS in protoplasts
528 transformed with ami*r*21), and *AT5G37600 (ARABIDOPSIS GLUTAMINE SYNTHASE 1)*
529 involved in nitrate assimilation, by 51%, and 16%, respectively (Figure 8 A).

530

531 **5'-RLM-RACE reveals non-canonical cleavage of Arabidopsis target genes in**
532 **protoplasts expressing *Si*sRNAs with preference for AGO1**

533 We selected *Si*sRNA24 to study the cleavage pattern of its significantly down-
534 regulated target transcripts *AT1G65090* and *AT4G15765* using 5'-RLM-RACE. For the
535 predicted target transcript *AT1G65090,* no band corresponding to an expected
536 canonical cleavage product was detected (Supplemental Figure 6A). For target
537 gene *AT4G15765*, we detected a single band of 300 bp in protoplasts expressing
538 *Si*sRNA24*,* which was shorter than the expected size (443 bp), while double bands
539 were observed for the control protoplasts. PCR amplicon from both transformed
540 and control protoplasts were cloned into the pGEM-T® cloning vector and
541 sequenced. Sequence analysis confirmed the alignment of the 300 bp RLM-RACE
542 product with *AT4G15765*. However, it did not confirm the 5´-end position, between
543 nt 10 and 11, predicted for *Sis*RNA24-guided canonical cleavage (Supplemental
544 Figure 6B). The absence of cleavage and/or a canonical cleavage product does not
545 exclude the potential of *Si*sRNA24 in mediating predicted *At* gene silencing as many
546 previous studies have highlighted the challenge of identifying sRNAs cleavage sites
547 in plants (Brousse *et al.,* 2014; Werner *et al.,* 2021).

548

549 **Predicted *Si*sRNAs effectors are loaded onto Arabidopsis AGO1**

550 To further substantiate the hypothesis that ckRNAi occurs in the interaction
551 between *Si* and *At* and that predicted *Si*sRNAs effectors are likely to be loaded into
552 the Arabidopsis RISC complex, we conducted *At*AGO1/sRNA co-
553 immunoprecipitation (Co-IP) using samples of *Si*-colonised roots, followed by
554 stem-loop PCR analysis (Carbonell, 2017b; Dunker *et al.,* 2021). To exclude the
555 possibility that the *At*-specific anti-AGO1 antibody would cross-react with fungal
556 AGOs, we first performed an *At*AGO1/sRNA Co-IP followed by Western-Blot (WB)
557 analysis using a 4-week-old *Si* axenic culture. No binding of the *At*AGO1-specific
558 antibody was detected in the crude extract neither in the supernatant nor in the
559 IP fraction in comparison to the total loaded proteins from *Si* axenic culture
560 confirming the specificity of the plant anti-AGO1 antibody (Supplementary Figure
561 7A). In line with this, no *Si*sRNAs could be detected by stem-loop PCR using *Si*sRNA-
562 specific stem-loop primers (Supplementary Figure 7B). Similarly, western Blot
563 analysis of *At*AGO1-IP of samples from *Si*-colonized *At* roots and *At* mock roots was
564 performed. AGO1 accumulation was observed in crude extracts and IP fractions
565 with a stronger signal in the IP fraction than in the supernatant from *Si-At* sample
566 (Figures 9A and 9B).
567
568 Next, from *Si*-colonized roots (*Si-At*) Co-IP we recovered the *At*AGO1-bound sRNA
569 sample. Stem-loop PCR was performed and detected the *At*AGO1-bound
570 AtmiR159a and a band of the expected size for *Si*sRNA21, *Si*sRNA23, *Si*sRNA24,
571 *Si*sRNA28 (Figure 10), whereas *At*miR393a*, which is known to preferably bind
572 *At*AGO2 (Mi *et al.,* 2008), was undetectable. Stem-loop PCR products from the *Si-At*
573 Co-IP fraction were cloned and sequenced. The sequencing results confirmed the
574 presence of plant *At*miR159a as well as *Si*sRNA2*4* and *Si*sRNA28 with the exact
575 same sequences detected from *Si* axenic culture and *Si*-colonized *At* roots
576 confirming the success of the pull-down. In addition, two *Si*sRNAs with almost
577 identical sequences to *Si*sRNA21 and *Si*sRNA23 were also co-immunoprecipitated
578 (Supplementary Table 10). Such mismatches that we detected for *Si*sRNA21 and

579 *Si*sRNA23 may be caused by the processing steps of the sRNAs until the loading
580 into the AGO1, which may result in sequence variations compared to the total
581 RNAseq performed in our previous work (Šečić *et al*, 2021). Nevertheless, these
582 results show that detected *Si*sRNAs are bound to *At*AGO1, supporting the notion
583 that *Si*sRNAs are transferred into *At* root cells during root colonisation and loaded
584 into the plant RNAi machinery.

585

586 **Discussion**

587 In this work, we developed an experimental pipeline for the analysis of putative
588 fungal sRNA effectors and investigated their role in host target gene silencing. We
589 have previously reported the identification and analysis of fungal sRNAs induced
590 in the interaction of the root endophyte *Serendipita indica* (*Si)* and *Brachypodium*
591 *distachyon* (Šečić *et al.,* 2021) termed ck-*Si*sRNAs. To bridge the gap between the
592 large amount of bioinformatic data available from this previous study and the
593 functional validation of the ck-*Si*sRNAs, we established here a rapid, simple and
594 reproducible roadmap for the validation of ck-*Si*sRNA using Arabidopsis transient
595 protoplast system. We first validated the effectiveness of our pipeline, by
596 expressing artificial microRNAs (amiRNAs) and ck-*Si*sRNA in Arabidopsis
597 protoplasts, confirmed their accumulation and their potential in inducing post-
598 transcriptional gene silencing of the model plant *Arabidopsis thaliana* predicted
599 target genes. Selected *Si*sRNAs were confirmed to be accumulated in *Si*-colonized
600 roots and by immunoprecipitation pull-down assay, we showed that *Si*sRNAs are
601 loaded into the plant RNAi machinery, confirming the translocation of *Si*sRNA
602 effectors into host cells. Using *At*AGO/sRNA co-IP we detected the two *Si*sRNAs,
603 *Si*sRNA24 and *Si*sRNA28 bound to *At*AGO1 supporting the ckRNAi hypothesis.
604 Additional *Si*sRNAs of 21 nt were identified in the *At*AGO1 Co-IP assay that had
605 some mismatches when compared to the *Si*sRNA detected in *Si* axenic culture and
606 *Si-At* interaction.

607 To test the functionality of the selected ck-*Si*sRNAs in the *Si-At* symbiosis, we
608 generated a plant expression construct under the 35S promotor for sRNA
609 expression in protoplasts based on the pUC18 backbone vector and *At*MIR390a
610 distal stem-loop which can generate 21 nt amiRNAs or *Si*sRNAs. The *At*MIR390a
611 precursor belongs to the MIR390 family, which is highly conserved and precisely
612 produced and processed in several plant species (Axtell *et al.,* 2006; Cuperus *et al.,*
613 2011). Carbonell et al (2014) tested the functionality of the *At*MIR390a-based
614 amiRNAs vector in repressing target transcript accumulation in Arabidopsis plants
615 using the plant vector pMDC32BAtMIR390a-B/c, which enables the directed
616 cloning of amiRNAs and their stable expression in dicotyledonous plants
617 (Carbonell *et al.,* 2014). Although MIR390 associates preferably with AGO7, the
618 association of *At*MIR390a-derived amiRNAs that have a 5´ U can be directed to
619 AGO1 (Carbonell et al., 2014; Carbonell, 2017b; Cuperus et al., 2010; Montgomery
620 et al., 2008). Conventionally, an sRNA-AGO1-mediated cleavage results in a
621 canonical cut between nucleotides 10 and 11 of the sRNA at the corresponding
622 mRNA site. This cleavage is a confirmation of sRNA loading into AGO1, formation
623 of the RISC complex and degradation of the mRNA target (Addo-Quaye *et al.*, 2009;
624 Huntzinger & Izaurralde, 2011). In our approach, we combined the advantages of
625 plant expression vectors and protoplast transient expression systems, both
626 considered as valuable tools, to study gene silencing and the molecular
627 mechanisms of RNAi in plants (Tyurin *et al.,* 2020). To confirm the effectiveness of
628 the transient protoplasts system, we first used artificial microRNAs (amiRNAs) with
629 almost a perfect match to *At's* predicted target transcript. Four amiRNAs, amir21,
630 amir24, amir154 and amir296 (Supplemental Table 2, were expressed in *At*
631 protoplasts. All amiRNAs induced a significant reduction in mRNA abundance of
632 their corresponding host-target transcripts, confirming their effective silencing
633 activity in *At* protoplasts. AmiRNAs used in our pipeline are algorithmically
634 designed to exhibit a 5' U, thereby enabling their loading into the AGO1 protein
635 (Carbonell, 2017c). Consequently, they can enter the RISC complex and induce a

636 downregulation of the target gene. We then investigated whether amir296 that
637 showed a reduction of 65% of the predicted target *AT2G45240* (MAP1A,
638 METHIONINE AMINOPEPTIDASE 1A), can mediate a canonical cleavage of the same
639 target *AT2G45240,* and indeed detected using 5'-RLM-RACE a cleavage site of the
640 mRNA transcript between position 10 and 11 of amir296 indicating that it can
641 induce a potential *At*AGO1-mediated degradation of *AT2G45240* mRNA.

642 Next, we expressed a set of the selected putative ck-*Si*sRNAs in Arabidopsis
643 protoplasts. The expression and accumulation of the putative *Si*sRNA24, exhibiting
644 a 5´-U, was validated by stem-loop PCR. Four of five predicted targets of *Si*sRNA24
645 showed a significantly reduced abundance in the transformed protoplasts.

646 Another putative *SisRNA*, *SisRNA154*, which also has a 5'-U, showed significant
647 downregulation only for the target *AT2G47600* from the two *At* predicted target
648 genes.

649 An important factor to consider when studying PTGS via sRNA effectors is the
650 degree of mismatches, expressed as "Expectation value" reporting on the
651 mismatch score between the predicted target mRNA and the sRNA. Previous
652 studies have demonstrated that the number and position of mismatches between
653 the sRNA and the corresponding target mRNA can significantly impact their
654 binding affinity, eventually weakening the interaction and resulting in either non-
655 significant or no downregulation (Carbonell et al., 2015; Ossowski et al., 2008;
656 Rhoades et al., 2002). Studies have shown that mismatches within the sRNA seed
657 region spanning nt 2 to 12/13 are possible, but they may reduce the sRNA activity,
658 whereas mismatches at position 1 or between nt 14 and 21 are more acceptable
659 (Carbonell, 2017a; Mallory *et al.*, 2004). Moreover, mismatches can also lead to a
660 different mode of action for the sRNA, and instead of an mRNA degradation
661 pathway, mismatches can trigger a deadenylation pathway or a translational
662 repression pathway, thus causing a decrease in protein synthesis instead of an
663 mRNA target degradation (Baulcombe, 2004; Carthew & Sontheimer, 2009). We

664 also hypothesize that a high abundance level of a target mRNA may lead to less
665 detectable downregulation, as its accessibility for the sRNA may have an impact
666 on the silencing process and the detection of a canonical cleavage. It is also
667 conceivable that the presence of other endogenous miRNAs, which may bind near
668 or at the same mRNA binding site might disrupt sRNA/mRNA binding, modulate
669 the regulatory outcome, and affect the gene expression pattern.

670 Further analysis of the molecular cleavage pattern of *Si*sRNA24 by 5´-RLM-RACE
671 identified noncanonical cut sites in the target gene *AT4G15765.* This finding may
672 be explained by the fact that cleavage products might be present at a low
673 abundance, falling below the detection threshold of the RLM-RACE method and
674 making the detection of a precise canonical cleavage a challenge. Alternatively, it
675 might be also possible that the cleavage site within the target mRNA could be
676 located at a different position. Moreover, 5´-RLM-RACE is a challenging method to
677 detect cleavage sites. High throughput sequencing of samples from the *Si-At*
678 interaction including transcriptional analysis and degradome sequencing are
679 needed to better understand *Si*sRNA-mediated target cleavage. Hence,
680 consideration for sRNA non-canonical cleavage site may be further investigated as
681 different studies speculate that PTGS can still be induced through sRNA or
682 phasiRNA and generate a non-canonical cleavage site (Brousse *et al*., 2014; Ivanova
683 *et al*., 2022).

684 In our study, the Arabidopsis target *AT5G25350* is predicted to be targeted by both
685 amir21 and *Si*sRNA21. When expressing amir21 (with 5´ U and an expectation
686 value of 0), the mRNA abundance of *AT5G25350* showed a downregulation of 68%.
687 However, when expressing *Si*sRNA21 (with a 5´C and an expectation value of 5)
688 we observed a downregulation of 51% of the same target gene. Another example
689 is the predicted target gene *AT4G32160* targeted by amir154 and *Si*sRNA154 both
690 with a 5´ U. The mRNA abundance of *AT4G32160* in protoplasts expressing
691 amir154 (with an expectation value of 0) resulted in a reduction of 50% but

692 protoplasts expressing *Si*sRNA154 (with an expectation value of 4.5) did not show
693 a reduction of *AT4G32160* transcript (Supplemental Figure 8). These results raise
694 the possibility that amiRNAs are more prone to mediate target gene silencing but
695 further studies with additional amiRNAs and putative sRNAs are required to
696 confirm these observations.

697 We extended our investigation by performing *At*AGO1/sRNA Co-IP on samples
698 from *Si*-colonized Arabidopsis roots and western-blot analysis confirmed the
699 enrichment of the *At*AGO1 in the IP fraction. We subsequently detected using
700 stem-loop PCR two ck-*Si*sRNAs: *Si*sRNA24 and *Si*sRNA28, bound to *At*AGO1
701 providing strong evidence of the translocation of *Si*sRNAs and their incorporation
702 into Arabidopsis RNAi machinery. Importantly, the identification in the *At*AGO1-IP
703 of two *Si*sRNAs exhibiting nucleotide variations at their 3´terminal end to the
704 previously identified ck-*Si*sRNA (*Si*sRNA21 and *Si*sRNA23) suggests alternative
705 *Si*sRNA variants. The presence of such variants highlights the complexity of the
706 sRNA-mediated regulatory networks during *Si*-host root colonization. Conducting
707 a high throughput sequencing of the entire pool of *Si*sRNA pulled down from
708 *At*AGO1 Co-IP could identify a large "Repertoire" of *Si*sRNAs effectors with a
709 functional role in *Si* symbiosis.

710 In conclusion, we have developed a transient protoplast expression system to
711 investigate the potential role of putative *Si*sRNA effectors in regulating target gene
712 expression in *Arabidopsis thaliana*. This validation tool will not only help to
713 understand the underlying molecular mechanism of *Si*sRNA-mediated PTGS but
714 will also allow us to examine ckRNAi in mutualistic plant-fungal association.

715 By studying *Si*sRNA-mediated PTGS, we have gained first insights into the
716 possibility that the endophytic fungus *Si* exploits sRNA effectors for the
717 establishment of its mutualistic symbiosis with plants. More targeted studies will
718 confirm whether *Si* utilizes its sRNAs to modulate the plant immune system and
719 identify more genes that can be silenced during the *Si-At* interaction. With the great

720 potential of *Si* to colonize a wide host range of plants, we expect that findings from
721 the study of the *Si-At* interaction can be translated to crop plants. Moreover,
722 amiRNAs have been shown to be effective in fine-tuning gene expression in plants
723 with a high silencing level (Carbonell et al., 2014; Cisneros & Carbonell, 2020).
724 Therefore, they can be viewed as a potential tool for RNAi-mediated crop
725 protection strategies. Computational tools, along with *in vivo* and *in vitro*
726 experimental setups, can expand our knowledge of ckRNAi and reveal the
727 unknown about mutualistic and pathogenic interaction for cost-effective basic
728 research and agronomic application.

729

730 **Figure legends**

731 **Figure 1. Flowchart showing the methods and outputs in this study.** The
732 turquoise colour indicates the different input material and purple indicates the
733 wet-lab steps. Green represents the validated outputs of the study. For details also
734 see Material and Methods. *Si*, *Serendipita indica*; *At*, *Arabidopsis thaliana*; PTGS,
735 post-transcriptional gene silencing; amiRNA, artificial miRNA.

736 **Figure 2. Duplexed stem-loop PCR confirming expression of amiRNAs in**
737 **Arabidopsis protoplasts.** Agarose gel analysis shows expression of all four
738 amiRNAs in transformed protoplasts 24 hours post-transformation (hptr), but not
739 in control protoplasts. Plant *At*miR159a of 21 nt length was used as a positive
740 control.

741 **Figure 3. qPCR analysis of target gene silencing in Arabidopsis protoplasts 24**
742 **h post transformation with amiRNAs.** The mRNA transcript levels in
743 transformed protoplasts (+) expressing amir21, amir24, amir154, and amir296
744 were normalized against housekeeping gene *Ubiquitin* (*AT3G62250*) and displayed
745 as fold change relative to control protoplasts (-) (mock-treated without amiRNA
746 construct). Data are the average of two to three biological replicates ± standard

747 deviation. Asterisks indicate difference at p ≤ 0.05 (*), p ≤ 0.01 (**), and p ≤ 0.001
748 (***) according to Student's t-test. ns= not significant.

749 **Figure 4.** Identification of 5'-RLM-RACE target sites in *AT2G45240* mRNA following
750 amir296 expression in Arabidopsis protoplasts **(A)** PCR products of the second
751 nested 5´-RLM-RACE-PCR visualized in an EtBr-agarose gel. RNA was extracted
752 from transformed protoplasts with amir296 (T) and from the corresponding
753 controls (control protoplasts (C) and non-treated protoplasts (NP). **(B)** Mapping of
754 *AT2G45240* target cleavage products by 5´-RLM-RACE. The predicted base pairing
755 between amir296 and *AT2G45240* is shown in green. The red arrow indicates the
756 detected canonical cleavage sites. The proportion of cloned 5´-RLM-RACE
757 products at the different cleavage sites is shown in brackets. For amir296
758 transformed protoplasts, three colonies have the 5´-end at the expected position,
759 opposite to nucleotides 10-11 of amir296, which is not the case for control and
760 non-treated protoplasts.

761 **Figure 5: Gel electrophoresis of products from stem-loop PCR analysis of a**
762 **set of potential *Si*sRNA effectors from *Serendipita indica*.** The *Si*RNAs were
763 selected from previous RNAseq data sets generated from the mutualistic
764 interaction of *Serendipita indica* and *Brachypodium distachyon* (Šečić *et al.,* 2021).
765 Multiplexed stem-loop PCR confirmed the presence of *Si*sRNAs in a 4-week-old *Si*
766 axenic culture. A PCR product of the expected size of 62 bp (sum of the 21 bp of
767 the sRNA sequence, loop region, plus the forward primer and the reverse primer
768 length) is visualized in a 2% agarose gel. The plant *At*miR159a of 21 nt long served
769 as a negative control. A weaker band of *Si*sRNA 296 was detected due to a lower
770 abundance of the sRNA in the sample (see supplemental Table 8). An unspecific
771 amplification (confirmed by Sanger sequencing) was detected for the *At*miR159a
772 due to the multiplexing of hairpin primers or a possible partial complementarity
773 of the hairpin primer to a non-target sequence.

774 **Figure 6: Detection of predicted *Si*sRNAs effectors in Arabidopsis roots**
775 **colonized by *Serendipita indica*. (A)** Root colonization pattern at 7 dpi.
776 Fluorescence microscopy shows green chitin-specific WGA-AF488 staining of
777 hyphal walls (λexc494 nm, λem515) **(B)** Detection of *Si*sRNAs in roots at 3-, 7- and
778 14 dpi using multiplexed stem-loop PCR. Agarose gel analysis of *Si*sRNA detected
779 bands of the expected size of 62 bp. Plant *At*miR159a was used as a positive control
780 for a plant-expressed sRNA.

781 **Figure 7. Duplexed stem-loop PCR confirming expression of *Si*sRNAs in**
782 **Arabidopsis protoplasts.** Agarose gel analysis of stem-loop PCR confirmed the
783 detection of all four expressed *Si*sRNA in transformed protoplasts 24 hptr, but not
784 in control protoplasts. Plant *At*miR159a was used as a positive control.

785 **Figure 8. qPCR analysis of target gene silencing in Arabidopsis protoplasts 24**
786 **hptr with *Si*sRNAs vs. control (protoplast without *Si*sRNA construct).** The
787 mRNA transcript levels in transformed protoplasts (+) expressing **(A)** *Si*sRNA21, **(B)**
788 *Si*sRNA24, **(C)** *Si*sRNA28, and **(D)** *Si*sRNA154 normalized against housekeeping
789 gene *Ubiquitin* (*AT3G62250*) are displayed as fold change relative to control
790 protoplasts. Data are the average of two to three biological replicates ± standard
791 deviation. Asterisks indicate difference at $p \leq 0.05$(*), $p \leq 0.01$ (**) and $p \leq 0.001$
792 (***) according to Student's t-test. ns= not significant.

793 **Figure 9. Quality control of AGO1 co-immunoprecipitation by western blot.**
794 Four sample fractions of the AGO1 co-IP experiment were analyzed: total protein
795 before centrifugation and debris removal, crude extract (CE) after centrifugation
796 and debris removal, supernatant (SN) after incubation with anti-*At*AGO1 and
797 agarose beads, and IP fraction (resuspended IP pellet). These four fractions were
798 analyzed in **(A)** *Si*-colonized root samples and **(B)** in *At* mock-treated roots. Both
799 figures show the detection of *At*AGO1 using anti-*At*AGO1-specific antibody at the
800 expected size of ~ 130 kDa. Note that AGO1 signals were stronger in IP fractions

than in SN. The broad-range pre-stained protein marker was used as a protein-size marker.

Figure 10: *Si*sRNAs co-immunoprecipitated with *At*AGO1 in *Si*-colonized Arabidopsis roots. Stem-loop PCR analysed in agarose gel confirms the presence of *Si*sRNA21, *Si*sRNA23, *Si*sRNA24, *Si*sRNA28, as well as AGO1 bound *At*miR159a but not AGO2 bound *At*miR393a* in *At*AGO1-co-IP samples from *Si*-colonized *At* roots.

Acknowledgments

The authors gratefully thank R. Eichmann for critically reading and correcting the manuscript. We thank M. Ladera-Carmona and B.T. Werner for their comments and suggestions. We thank the German Research Foundation (DFG) for supporting our research on RNA in plant-pathogen interactions by granting the DFG research unit RU5116 on exRNA to KHK. SN is supported by the Dr. Ernst-Leopold Klipstein-Stiftung, Paderborn, Giessen.

Conflict of interest

The authors declare that they have no competing interests.

Author contributions

S.N. and J.S. conceived the study; S.N. and K-H.K. wrote the paper; J.S. and E. Š. generated prediction of Arabidopsis targets from sRNAseq data. S.N., K.B., and S.S. conducted the functional experiments. All authors read and approved the final manuscript.

828 ## References

829 Addo-Quaye, C., Snyder, J. A., Park, Y. B., Li, Y.-F., Sunkar, R., & Axtell, M. J. (2009). Sliced microRNA
830 targets and precise loop-first processing of MIR319 hairpins revealed by analysis of the
831 Physcomitrella patens degradome. *RNA*, *15*(12), 2112–2121.
832 https://doi.org/10.1261/rna.1774909

833 Adhikari, S., Turner, M., & Subramanian, S. (2013). Hairpin Priming Is Better Suited than In Vitro
834 Polyadenylation to Generate cDNA for Plant miRNA qPCR. *Molecular Plant*, *6*(1), 229–231.
835 https://doi.org/10.1093/mp/sss106

836 Akum, F. N., Steinbrenner, J., Biedenkopf, D., Imani, J., & Kogel, K.-H. (2015). The Piriformospora
837 indica effector PIIN_08944 promotes the mutualistic Sebacinalean symbiosis. *Frontiers in*
838 *Plant Science*, *6*, 906. https://doi.org/10.3389/fpls.2015.00906

839 Axtell, M. J., Jan, C., Rajagopalan, R., & Bartel, D. P. (2006). A Two-Hit Trigger for siRNA Biogenesis in
840 Plants. *Cell*, *127*(3), 565–577. https://doi.org/10.1016/j.cell.2006.09.032

841 Bargmann, B. O. R., & Birnbaum, K. D. (2009). Positive Fluorescent Selection Permits Precise, Rapid,
842 and In-Depth Overexpression Analysis in Plant Protoplasts. *Plant Physiology*, *149*(3), 1231–
843 1239. https://doi.org/10.1104/pp.108.133975

844 Baulcombe, D. (2004). RNA silencing in plants. *Nature*, *431*(7006), Article 7006.
845 https://doi.org/10.1038/nature02874

846 Brousse, C., Liu, Q., Beauclair, L., Deremetz, A., Axtell, M. J., & Bouché, N. (2014). A non-canonical
847 plant microRNA target site. *Nucleic Acids Research*, *42*(8), 5270–5279.
848 https://doi.org/10.1093/nar/gku157

849 Cai, Q., Qiao, L., Wang, M., He, B., Lin, F.-M., Palmquist, J., Huang, S.-D., & Jin, H. (2018). Plants send
850 small RNAs in extracellular vesicles to fungal pathogen to silence virulence genes. *Science*
851 *(New York, N.Y.)*, *360*(6393), 1126–1129. https://doi.org/10.1126/science.aar4142

852 Carbonell, A. (2017a). Artificial small RNA-based strategies for effective and specific gene silencing in
853 plants. *Plant Gene Silencing: Mechanisms and Applications*, 110–127.
854 https://doi.org/10.1079/9781780647678.0110
855 Carbonell, A. (2017b). Immunoprecipitation and High-Throughput Sequencing of ARGONAUTE-Bound
856 Target RNAs from Plants. In A. Carbonell (Ed.), *Plant Argonaute Proteins: Methods and*
857 *Protocols* (pp. 93–112). Springer. https://doi.org/10.1007/978-1-4939-7165-7_6
858 Carbonell, A. (2017c). Plant ARGONAUTEs: Features, Functions, and Unknowns. In A. Carbonell (Ed.),
859 *Plant Argonaute Proteins: Methods and Protocols* (pp. 1–21). Springer.
860 https://doi.org/10.1007/978-1-4939-7165-7_1
861 Carbonell, A., Fahlgren, N., Mitchell, S., Cox Jr, K., Mockler, T., & Carrington, J. (2015). Highly Specific
862 Gene Silencing in a Monocot Species by Artificial MicroRNAs Derived From Chimeric MIRNA
863 Precursors. *Plant J. (in Press)*. https://doi.org/10.1111/tpj.12835
864 Carbonell, A., Takeda, A., Fahlgren, N., Johnson, S. C., Cuperus, J. T., & Carrington, J. C. (2014). New
865 generation of artificial MicroRNA and synthetic trans-acting small interfering RNA vectors for
866 efficient gene silencing in Arabidopsis. *Plant Physiology*, *165*(1), 15–29.
867 https://doi.org/10.1104/pp.113.234989
868 Carthew, R. W., & Sontheimer, E. J. (2009). Origins and Mechanisms of miRNAs and siRNAs. *Cell*,
869 *136*(4), 642–655. https://doi.org/10.1016/j.cell.2009.01.035
870 Cisneros, A. E., & Carbonell, A. (2020). Artificial Small RNA-Based Silencing Tools for Antiviral
871 Resistance in Plants. *Plants*, *9*(6), Article 6. https://doi.org/10.3390/plants9060669
872 Colombo, S., Nielsen, H. M., & Foged, C. (2013). Evaluation of carrier-mediated siRNA delivery:
873 Lessons for the design of a stem-loop qPCR-based approach for quantification of intracellular
874 full-length siRNA. *Journal of Controlled Release*, *166*(3), 220–226.
875 https://doi.org/10.1016/j.jconrel.2013.01.006
876 Cuperus, J. T., Carbonell, A., Fahlgren, N., Garcia-Ruiz, H., Burke, R. T., Takeda, A., Sullivan, C. M.,
877 Gilbert, S. D., Montgomery, T. A., & Carrington, J. C. (2010). Unique Functionality of 22 nt

878 miRNAs in Triggering RDR6-Dependent siRNA Biogenesis from Target Transcripts in
879 Arabidopsis. *Nature Structural & Molecular Biology*, *17*(8), 997–1003.
880 https://doi.org/10.1038/nsmb.1866
881 Cuperus, J. T., Fahlgren, N., & Carrington, J. C. (2011). Evolution and Functional Diversification of
882 MIRNA Genes. *The Plant Cell*, *23*(2), 431–442. https://doi.org/10.1105/tpc.110.082784
883 Dai, X., Zhuang, Z., & Zhao, P. X. (2018). psRNATarget: A plant small RNA target analysis server (2017
884 release). *Nucleic Acids Research*, *46*(Web Server issue), W49–W54.
885 https://doi.org/10.1093/nar/gky316
886 Dunker, F., Lederer, B., & Weiberg, A. (2021). Plant ARGONAUTE Protein Immunopurification for
887 Pathogen Cross Kingdom Small RNA Analysis. *Bio-Protocol*, *11*(3), e3911.
888 https://doi.org/10.21769/BioProtoc.3911
889 Fahlgren, N., Hill, S. T., Carrington, J. C., & Carbonell, A. (2016). P-SAMS: A web site for plant artificial
890 microRNA and synthetic trans-acting small interfering RNA design. *Bioinformatics*, *32*(1),
891 157–158. https://doi.org/10.1093/bioinformatics/btv534
892 Glaeser, S. P., Imani, J., Alabid, I., Guo, H., Kumar, N., Kämpfer, P., Hardt, M., Blom, J., Goesmann, A.,
893 Rothballer, M., Hartmann, A., & Kogel, K.-H. (2016). Non-pathogenic Rhizobium radiobacter
894 F4 deploys plant beneficial activity independent of its host Piriformospora indica. *The ISME*
895 *Journal*, *10*(4), 871–884. https://doi.org/10.1038/ismej.2015.163
896 Göhre, V., & Weiberg, A. (2023). RNA Dialogues in Fungal–Plant Relationships. In B. Scott & C.
897 Mesarich (Eds.), *Plant Relationships: Fungal-Plant Interactions* (pp. 31–51). Springer
898 International Publishing. https://doi.org/10.1007/978-3-031-16503-0_2
899 He, B., Cai, Q., Qiao, L., Huang, C.-Y., Wang, S., Miao, W., Ha, T., Wang, Y., & Jin, H. (2021). RNA-
900 binding proteins contribute to small RNA loading in plant extracellular vesicles. *Nature*
901 *Plants*, *7*(3), 342–352. https://doi.org/10.1038/s41477-021-00863-8
902 He, B., Hamby, R., & Jin, H. (2021). Plant extracellular vesicles: Trojan horses of cross-kingdom
903 warfare. *FASEB BioAdvances*, *3*(9), 657–664. https://doi.org/10.1096/fba.2021-00040

904 Huang, G., Allen, R., Davis, E. L., Baum, T. J., & Hussey, R. S. (2006). Engineering broad root-knot
905 resistance in transgenic plants by RNAi silencing of a conserved and essential root-knot
906 nematode parasitism gene. *Proceedings of the National Academy of Sciences*, *103*(39),
907 14302–14306. https://doi.org/10.1073/pnas.0604698103
908 Huntzinger, E., & Izaurralde, E. (2011). Gene silencing by microRNAs: Contributions of translational
909 repression and mRNA decay. *Nature Reviews Genetics*, *12*(2), Article 2.
910 https://doi.org/10.1038/nrg2936
911 Ivanova, Z., Minkov, G., Gisel, A., Yahubyan, G., Minkov, I., Toneva, V., & Baev, V. (2022). The
912 Multiverse of Plant Small RNAs: How Can We Explore It? *International Journal of Molecular*
913 *Sciences*, *23*(7), 3979. PubMed. https://doi.org/10.3390/ijms23073979
914 Iwakawa, H., & Tomari, Y. (2022). Life of RISC: Formation, action, and degradation of RNA-induced
915 silencing complex. *Molecular Cell*, *82*(1), 30–43.
916 https://doi.org/10.1016/j.molcel.2021.11.026
917 Koch, A., Kumar, N., Weber, L., Keller, H., Imani, J., & Kogel, K.-H. (2013). Host-induced gene silencing
918 of cytochrome P450 lanosterol C14α-demethylase–encoding genes confers strong resistance
919 to Fusarium species. *Proceedings of the National Academy of Sciences*, *110*(48), 19324–
920 19329. https://doi.org/10.1073/pnas.1306373110
921 Kramer, M. F. (2011). STEM-LOOP RT-qPCR for miRNAS. *Current Protocols in Molecular Biology /*
922 *Edited by Frederick M. Ausubel ... [et Al.]*, *CHAPTER*, Unit15.10.
923 https://doi.org/10.1002/0471142727.mb1510s95
924 Lincoln, C., Britton, J. H., & Estelle, M. (1990). Growth and development of the axr1 mutants of
925 Arabidopsis. *The Plant Cell*, *2*(11), 1071–1080.
926 Liu, S., Jaouannet, M., Dempsey, D. A., Imani, J., Coustau, C., & Kogel, K.-H. (2020). RNA-based
927 technologies for insect control in plant production. *Biotechnology Advances*, *39*, 107463.
928 https://doi.org/10.1016/j.biotechadv.2019.107463

929 Livak, K. J., & Schmittgen, T. D. (2001). Analysis of relative gene expression data using real-time
930 quantitative PCR and the 2(-Delta Delta C(T)) Method. *Methods (San Diego, Calif.)*, *25*(4),
931 402–408. https://doi.org/10.1006/meth.2001.1262
932 Llave, C., Xie, Z., Kasschau, K. D., & Carrington, J. C. (2002). Cleavage of Scarecrow-like mRNA Targets
933 Directed by a Class of Arabidopsis miRNA. *Science*, *297*(5589), 2053–2056.
934 https://doi.org/10.1126/science.1076311
935 Mahanty, B., Mishra, R., & Joshi, R. K. (2023). Cross-kingdom small RNA communication between
936 plants and fungal phytopathogens-recent updates and prospects for future agriculture. *RNA*
937 *Biology*, *20*(1), 109–119. https://doi.org/10.1080/15476286.2023.2195731
938 Mallory, A. C., Reinhart, B. J., Jones-Rhoades, M. W., Tang, G., Zamore, P. D., Barton, M. K., & Bartel,
939 D. P. (2004). MicroRNA control of PHABULOSA in leaf development: Importance of pairing to
940 the microRNA 5′ region. *The EMBO Journal*, *23*(16), 3356–3364.
941 https://doi.org/10.1038/sj.emboj.7600340
942 Meyers, B. C., & Axtell, M. J. (2019). MicroRNAs in Plants: Key Findings from the Early Years. *The*
943 *Plant Cell*, *31*(6), 1206–1207. https://doi.org/10.1105/tpc.19.00310
944 Mi, S., Cai, T., Hu, Y., Chen, Y., Hodges, E., Ni, F., Wu, L., Li, S., Zhou, H., Long, C., Chen, S., Hannon, G.
945 J., & Qi, Y. (2008). Sorting of Small RNAs into Arabidopsis Argonaute Complexes Is Directed by
946 the 5′ Terminal Nucleotide. *Cell*, *133*(1), 116–127. https://doi.org/10.1016/j.cell.2008.02.034
947 Montgomery, T. A., Howell, M. D., Cuperus, J. T., Li, D., Hansen, J. E., Alexander, A. L., Chapman, E. J.,
948 Fahlgren, N., Allen, E., & Carrington, J. C. (2008). Specificity of ARGONAUTE7-miR390
949 interaction and dual functionality in TAS3 trans-acting siRNA formation. *Cell*, *133*(1), 128–
950 141. https://doi.org/10.1016/j.cell.2008.02.033
951 Moreno, P., Fexova, S., George, N., Manning, J. R., Miao, Z., Mohammed, S., Muñoz-Pomer, A.,
952 Fullgrabe, A., Bi, Y., Bush, N., Iqbal, H., Kumbham, U., Solovyev, A., Zhao, L., Prakash, A.,
953 García-Seisdedos, D., Kundu, D. J., Wang, S., Walzer, M., … Papatheodorou, I. (2022).

954 Expression Atlas update: Gene and protein expression in multiple species. *Nucleic Acids*
955 *Research*, *50*(D1), D129–D140. https://doi.org/10.1093/nar/gkab1030
956 Nasfi, S., & Kogel, K.-H. (2022). Packaged or unpackaged: Appearance and transport of extracellular
957 noncoding RNAs in the plant apoplast. *ExRNA; Vol 4 (May 31, 2022): ExRNA*.
958 https://exrna.amegroups.com/article/view/64855
959 Nowara, D., Gay, A., Lacomme, C., Shaw, J., Ridout, C., Douchkov, D., Hensel, G., Kumlehn, J., &
960 Schweizer, P. (2010). HIGS: Host-Induced Gene Silencing in the Obligate Biotrophic Fungal
961 Pathogen *Blumeria graminis*. *The Plant Cell*, *22*(9), 3130–3141.
962 https://doi.org/10.1105/tpc.110.077040
963 Osborne, R., Rehneke, L., Lehmann, S., Roberts, J., Altmann, M., Altmann, S., Zhang, Y., Köpff, E.,
964 Dominguez-Ferreras, A., Okechukwu, E., Sergaki, C., Rich-Griffin, C., Ntoukakis, V., Eichmann,
965 R., Shan, W., Falter-Braun, P., & Schäfer, P. (2023). Symbiont-host interactome mapping
966 reveals effector-targeted modulation of hormone networks and activation of growth
967 promotion. *Nature Communications*, *14*(1), Article 1. https://doi.org/10.1038/s41467-023-
968 39885-5
969 Ossowski, S., Schwab, R., & Weigel, D. (2008). Gene silencing in plants using artificial microRNAs and
970 other small RNAs. *The Plant Journal*, *53*(4), 674–690. https://doi.org/10.1111/j.1365-
971 313X.2007.03328.x
972 Qiang, X., Weiss, M., Kogel, K.-H., & Schäfer, P. (2012). Piriformospora indica—A mutualistic
973 basidiomycete with an exceptionally large plant host range. *Molecular Plant Pathology*,
974 *13*(5), 508–518. https://doi.org/10.1111/j.1364-3703.2011.00764.x
975 Qiao, S. A., Gao, Z., & Roth, R. (2023). A perspective on cross-kingdom RNA interference in
976 mutualistic symbioses. *New Phytologist*, *240*(1), 68–79. https://doi.org/10.1111/nph.19122
977 Reinhart, B. J., Weinstein, E. G., Rhoades, M. W., Bartel, B., & Bartel, D. P. (2002). MicroRNAs in
978 plants. *Genes & Development*, *16*(13), 1616–1626. https://doi.org/10.1101/gad.1004402

979 Ren, B., Wang, X., Duan, J., & Ma, J. (2019). Rhizobial tRNA-derived small RNAs are signal molecules
980 regulating plant nodulation. *Science (New York, N.Y.)*, *365*(6456), 919–922.
981 https://doi.org/10.1126/science.aav8907
982 Rhoades, M. W., Reinhart, B. J., Lim, L. P., Burge, C. B., Bartel, B., & Bartel, D. P. (2002). Prediction of
983 Plant MicroRNA Targets. *Cell*, *110*(4), 513–520. https://doi.org/10.1016/S0092-
984 8674(02)00863-2
985 Rutter, B. D., & Innes, R. W. (2018). Extracellular vesicles as key mediators of plant–microbe
986 interactions. *Current Opinion in Plant Biology*, *44*, 16–22.
987 https://doi.org/10.1016/j.pbi.2018.01.008
988 Sang, H., & Kim, J.-I. (2020). Advanced strategies to control plant pathogenic fungi by host-induced
989 gene silencing (HIGS) and spray-induced gene silencing (SIGS). *Plant Biotechnology Reports*,
990 *14*(1), 1–8. https://doi.org/10.1007/s11816-019-00588-3
991 Šečić, E., Zanini, S., Wibberg, D., Jelonek, L., Busche, T., Kalinowski, J., Nasfi, S., Thielmann, J., Imani,
992 J., Steinbrenner, J., & Kogel, K.-H. (2021). A novel plant-fungal association reveals
993 fundamental sRNA and gene expression reprogramming at the onset of symbiosis. *BMC*
994 *Biology*, *19*(1), 171. https://doi.org/10.1186/s12915-021-01104-2
995 Silvestri, A., Fiorilli, V., Miozzi, L., Accotto, G. P., Turina, M., & Lanfranco, L. (2019). In silico analysis of
996 fungal small RNA accumulation reveals putative plant mRNA targets in the symbiosis
997 between an arbuscular mycorrhizal fungus and its host plant. *BMC Genomics*, *20*, 169.
998 https://doi.org/10.1186/s12864-019-5561-0
999 Takeda, A., Iwasaki, S., Watanabe, T., Utsumi, M., & Watanabe, Y. (2008). The Mechanism Selecting
1000 the Guide Strand from Small RNA Duplexes is Different Among Argonaute Proteins. *Plant and*
1001 *Cell Physiology*, *49*(4), 493–500. https://doi.org/10.1093/pcp/pcn043
1002 Tyurin, A. A., Suhorukova, A. V., Kabardaeva, K. V., & Goldenkova-Pavlova, I. V. (2020). Transient
1003 Gene Expression is an Effective Experimental Tool for the Research into the Fine Mechanisms

1004 of Plant Gene Function: Advantages, Limitations, and Solutions. *Plants*, *9*(9), 1187.
1005 https://doi.org/10.3390/plants9091187
1006 Ueno, D., Yamasaki, S., & Kato, K. (2022). Methods for detecting RNA degradation intermediates in
1007 plants. *Plant Science*, *318*, 111241. https://doi.org/10.1016/j.plantsci.2022.111241
1008 Varkonyi-Gasic, E., & Hellens, R. P. (2011). Quantitative stem-loop RT-PCR for detection of
1009 microRNAs. *Methods in Molecular Biology (Clifton, N.J.)*, *744*, 145–157.
1010 https://doi.org/10.1007/978-1-61779-123-9_10
1011 Verma, N., Narayan, O. P., Prasad, D., Jogawat, A., Panwar, S. L., Dua, M., & Johri, A. K. (2022).
1012 Functional characterization of a high-affinity iron transporter (PiFTR) from the endophytic
1013 fungus Piriformospora indica and its role in plant growth and development. *Environmental*
1014 *Microbiology*, *24*(2), 689–706. https://doi.org/10.1111/1462-2920.15659
1015 Verma, S., Varma, A., Rexer, K.-H., Hassel, A., Kost, G., Sarbhoy, A., Bisen, P., Bütehorn, B., & Franken,
1016 P. (1998). Piriformospora indica, gen. Et sp. Nov., a new root-colonizing fungus. *Mycologia*,
1017 *90*(5), 896–903. https://doi.org/10.1080/00275514.1998.12026983
1018 Wang, M., & Dean, R. A. (2020). Movement of small RNAs in and between plants and fungi.
1019 *Molecular Plant Pathology*, *21*(4), 589–601. https://doi.org/10.1111/mpp.12911
1020 Wang, M., Thomas, N., & Jin, H. (2017). Cross-kingdom RNA trafficking and environmental RNAi for
1021 powerful innovative pre- and post-harvest plant protection. *Current Opinion in Plant Biology*,
1022 *38*, 133–141. https://doi.org/10.1016/j.pbi.2017.05.003
1023 Weiberg, A., Wang, M., Lin, F.-M., Zhao, H., Zhang, Z., Kaloshian, I., Huang, H.-D., & Jin, H. (2013).
1024 Fungal small RNAs suppress plant immunity by hijacking host RNA interference pathways.
1025 *Science (New York, N.Y.)*, *342*(6154), 118–123. https://doi.org/10.1126/science.1239705
1026 Weiß, M., Waller, F., Zuccaro, A., & Selosse, M.-A. (2016). Sebacinales – one thousand and one
1027 interactions with land plants. *New Phytologist*, *211*(1), 20–40.
1028 https://doi.org/10.1111/nph.13977

1029 Werner, B. T., Koch, A., Šečić, E., Engelhardt, J., Jelonek, L., Steinbrenner, J., & Kogel, K.-H. (2021).
1030 Fusarium graminearum DICER-like-dependent sRNAs are required for the suppression of host
1031 immune genes and full virulence. *PLOS ONE*, *16*(8), e0252365.
1032 https://doi.org/10.1371/journal.pone.0252365
1033 Wong-Bajracharya, J., Singan, V. R., Monti, R., Plett, K. L., Ng, V., Grigoriev, I. V., Martin, F. M.,
1034 Anderson, I. C., & Plett, J. M. (2022). The ectomycorrhizal fungus Pisolithus microcarpus
1035 encodes a microRNA involved in cross-kingdom gene silencing during symbiosis. *Proceedings*
1036 *of the National Academy of Sciences of the United States of America*, *119*(3), e2103527119.
1037 https://doi.org/10.1073/pnas.2103527119
1038 Wu, F.-H., Shen, S.-C., Lee, L.-Y., Lee, S.-H., Chan, M.-T., & Lin, C.-S. (2009). Tape-Arabidopsis
1039 Sandwich—A simpler Arabidopsis protoplast isolation method. *Plant Methods*, *5*(1), 16.
1040 https://doi.org/10.1186/1746-4811-5-16
1041 Xu, L., Wu, C., Oelmüller, R., & Zhang, W. (2018). Role of Phytohormones in Piriformospora indica-
1042 Induced Growth Promotion and Stress Tolerance in Plants: More Questions Than Answers.
1043 *Frontiers in Microbiology*, *9*. https://www.frontiersin.org/articles/10.3389/fmicb.2018.01646
1044 Yoo, S.-D., Cho, Y.-H., & Sheen, J. (2007). Arabidopsis mesophyll protoplasts: A versatile cell system
1045 for transient gene expression analysis. *Nature Protocols*, *2*(7), 1565–1572.
1046 https://doi.org/10.1038/nprot.2007.199
1047 Zand Karimi, H., & Innes, R. W. (2022). Molecular mechanisms underlying host-induced gene
1048 silencing. *The Plant Cell*, *34*(9), 3183–3199. https://doi.org/10.1093/plcell/koac165
1049 Zhan, J., & Meyers, B. C. (2023). Plant Small RNAs: Their Biogenesis, Regulatory Roles, and Functions.
1050 *Annual Review of Plant Biology*, *74*(1), 21–51. https://doi.org/10.1146/annurev-arplant-
1051 070122-035226
1052 Zhang, T., Zhao, Y.-L., Zhao, J.-H., Wang, S., Jin, Y., Chen, Z.-Q., Fang, Y.-Y., Hua, C.-L., Ding, S.-W., &
1053 Guo, H.-S. (2016). Cotton plants export microRNAs to inhibit virulence gene expression in a
1054 fungal pathogen. *Nature Plants*, *2*(10), 16153. https://doi.org/10.1038/nplants.2016.153

1055 Zuccaro, A., Lahrmann, U., Güldener, U., Langen, G., Pfiffi, S., Biedenkopf, D., Wong, P., Samans, B.,
1056 Grimm, C., Basiewicz, M., Murat, C., Martin, F., & Kogel, K.-H. (2011). Endophytic Life
1057 Strategies Decoded by Genome and Transcriptome Analyses of the Mutualistic Root
1058 Symbiont Piriformospora indica. *PLOS Pathogens*, *7*(10), e1002290.
1059 https://doi.org/10.1371/journal.ppat.1002290
1060

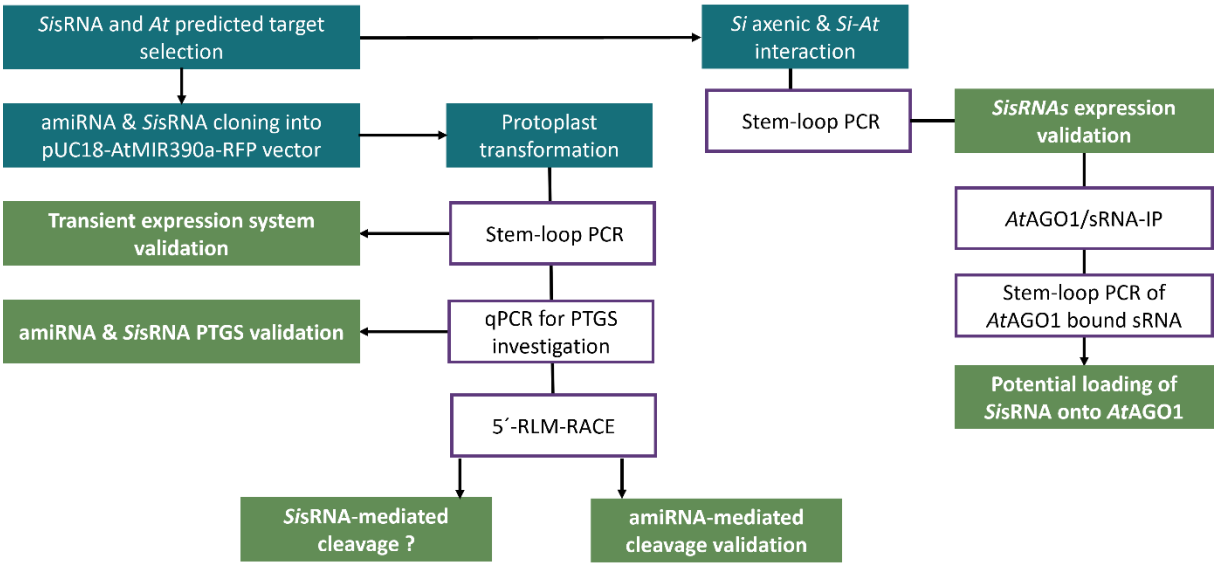

Figure 1. Flowchart showing the methods and outputs in this study. The turquoise colour indicates the different input material and purple indicates the wet-lab steps. Green represents the validated outputs of the study. For details also see Material and Methods. *Si*, *Serendipita indica*; *At*, *Arabidopsis thaliana*; PTGS, post-transcriptional gene silencing; amiRNA, artificial miRNA.

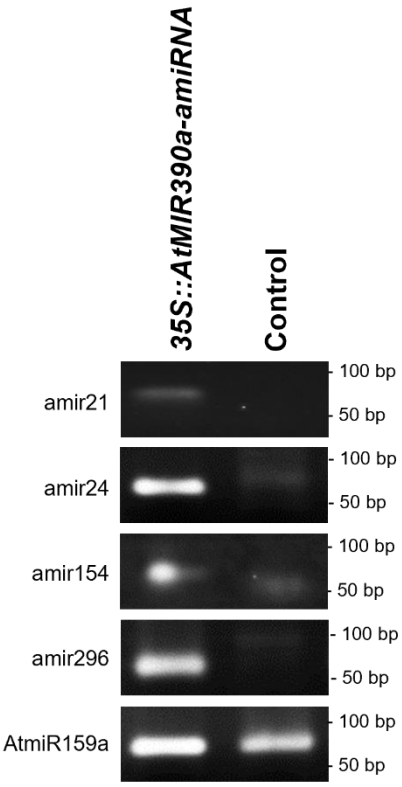

Figure 2. Duplexed stem-loop PCR confirming expression of amiRNAs in Arabidopsis protoplasts. Agarose gel analysis shows expression of all four amiRNAs in transformed protoplasts 24 hours post-transformation (hptr), but not in control protoplasts. Plant *At*miR159a of 21 nt length was used as a positive control.

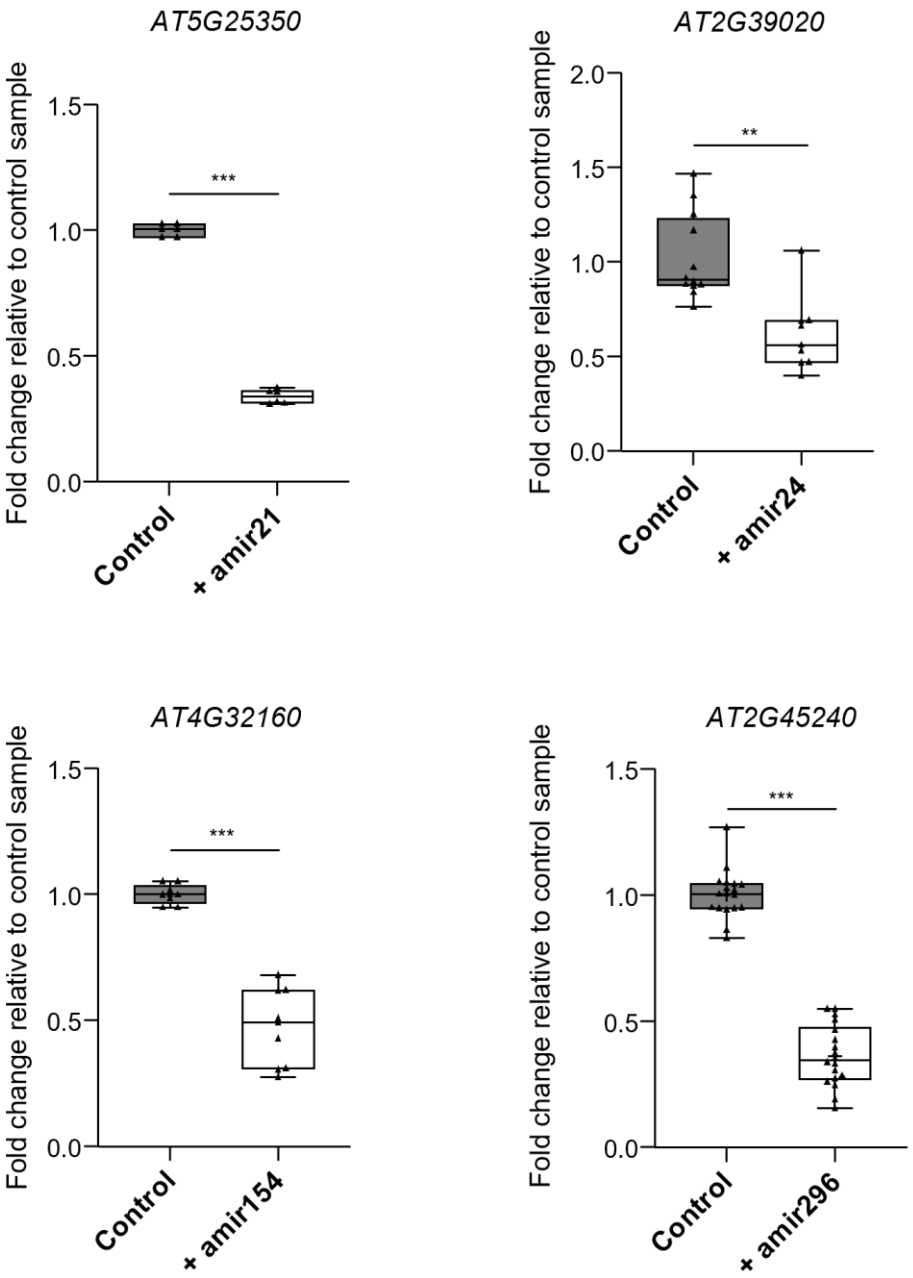

Figure 3. qPCR analysis of target gene silencing in Arabidopsis protoplasts 24 h post transformation with amiRNAs. The mRNA transcript levels in transformed protoplasts (+) expressing amir21, amir24, amir154, and amir296 were normalized against housekeeping gene *Ubiquitin* (*AT3G62250*) and displayed as fold change relative to control protoplasts (-) (mock-treated without amiRNA construct). Data are the average of two to three biological replicates ± standard

deviation. Asterisks indicate difference at p ≤ 0.05 (*), p ≤ 0.01 (**) and p ≤ 0.001 (***) according to Student's t-test. ns= not significant.

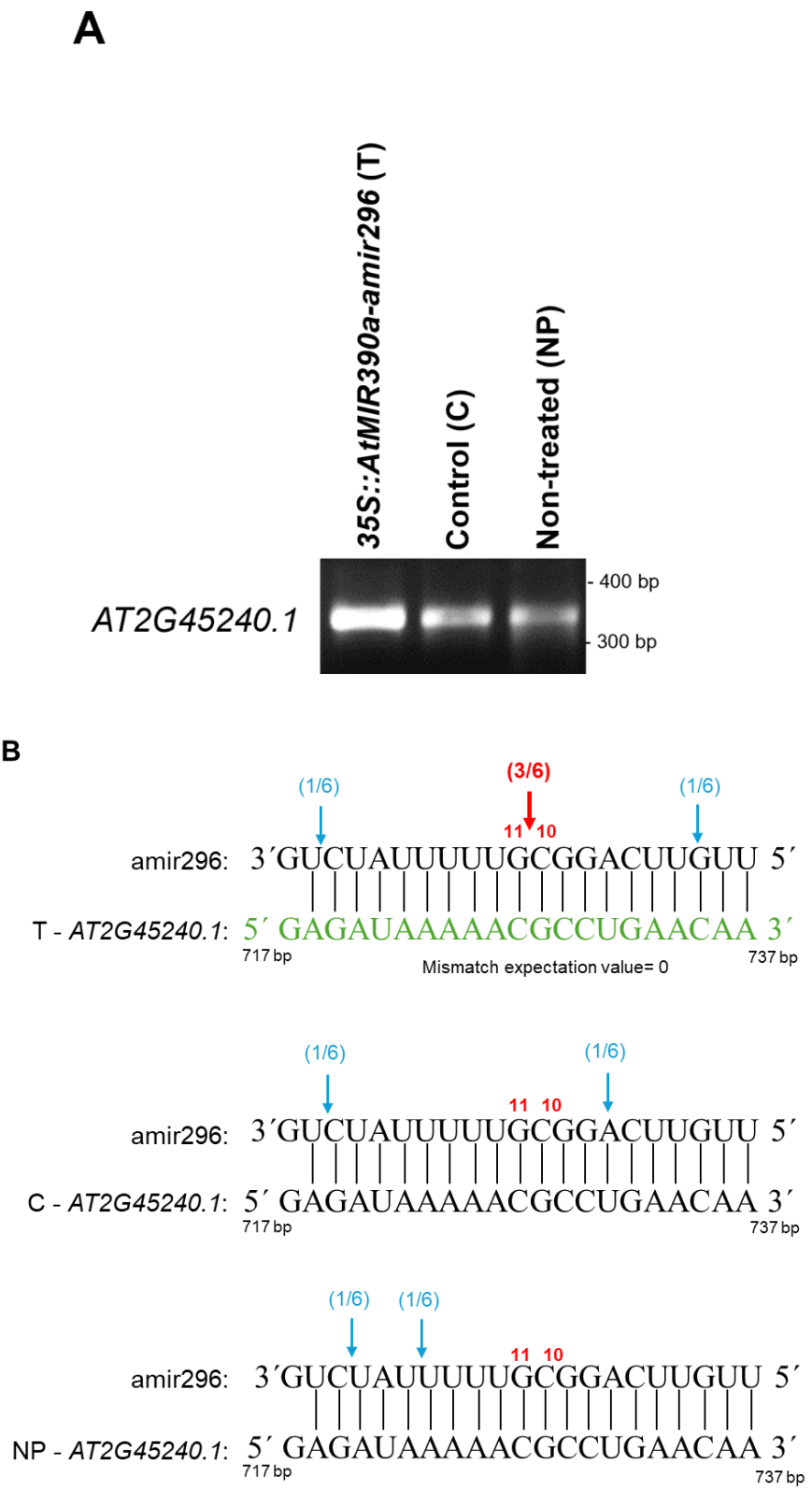

Figure 4. Identification of 5'-RLM-RACE target sites in *AT2G45240* mRNA following amir296 expression in Arabidopsis protoplasts **(A)** PCR products of the second nested 5´-RLM-RACE-PCR visualized in an EtBr-agarose gel. RNA was extracted from transformed protoplasts with amir296 (T) and from the corresponding controls (control protoplasts (C) and non-treated protoplasts (NP). **(B)** Mapping of *AT2G45240* target cleavage products by 5´-RLM-RACE. The predicted base pairing between amir296 and *AT2G45240* is shown in green. The red arrow indicates the detected canonical cleavage sites. The proportion of cloned 5´-RLM-RACE products at the different cleavage sites is shown in brackets. For amir296 transformed protoplasts, three colonies have the 5´-end at the expected position, opposite to nucleotides 10-11 of amir296, which is not the case for control and non-treated protoplasts.

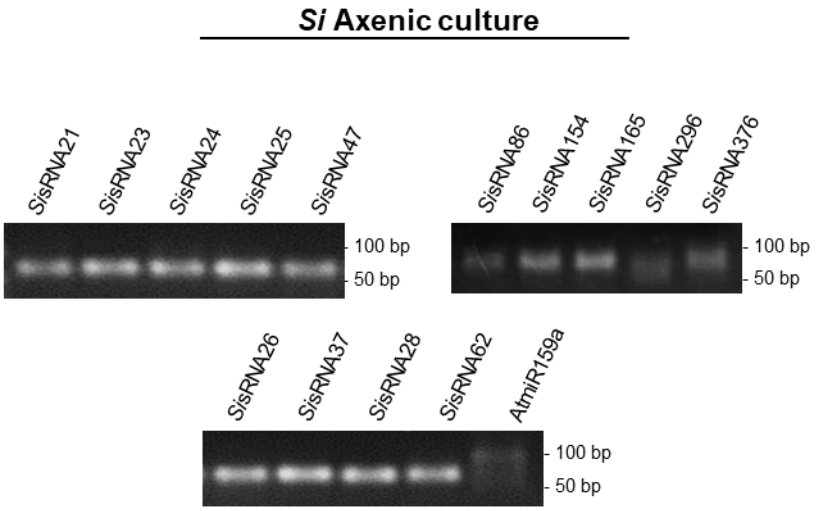

Figure 5: Gel electrophoresis of products from stem-loop PCR analysis of a set of potential *Si*sRNA effectors from *Serendipita indica*. The *Si*RNAs were selected from previous RNAseq data sets generated from the mutualistic interaction of *Serendipita indica* and *Brachypodium distachyon* (Šečić *et al.,* 2021).

Multiplexed stem-loop PCR confirmed the presence of *Si*sRNAs in a 4-week-old *Si* axenic culture. A PCR product of the expected size of 62 bp (sum of the 21 bp of the sRNA sequence, loop region, plus the forward primer and the reverse primer length) is visualized in a 2% agarose gel. The plant *At*miR159a of 21 nt long served as a negative control. A weaker band of *Si*sRNA 296 was detected due to a lower abundance of the sRNA in the sample (see supplemental Table 8). An unspecific amplification (confirmed by Sanger sequencing) was detected for the *At*miR159a due to the multiplexing of hairpin primers or a possible partial complementarity of the hairpin primer to a non-target sequence.

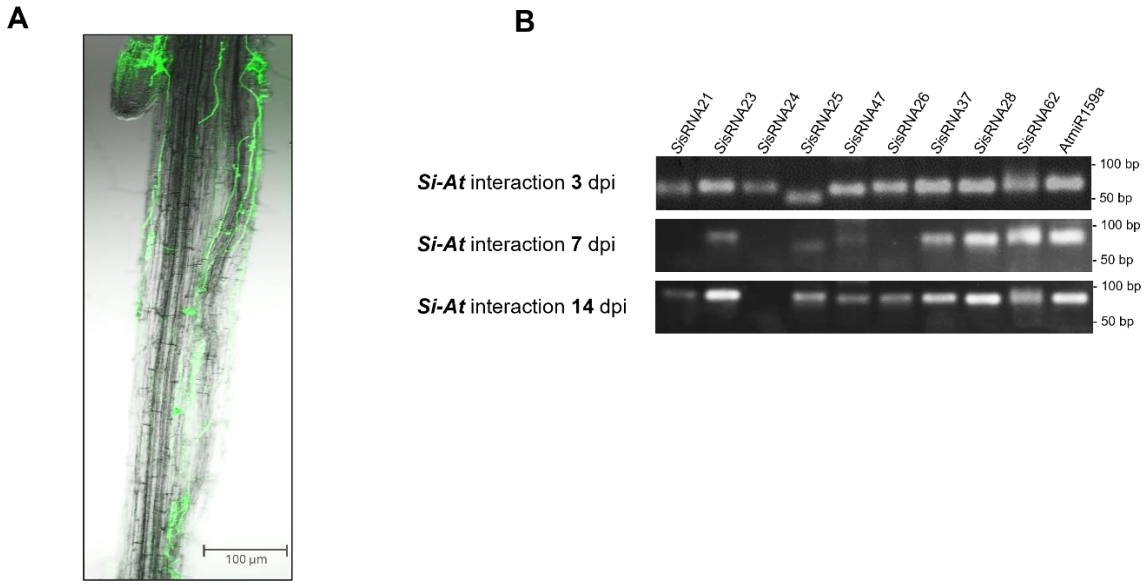

Figure 6: Detection of predicted *Si*sRNAs effectors in Arabidopsis roots colonized by *Serendipita indica*. (A) Root colonization pattern at 7 dpi. Fluorescence microscopy shows green chitin-specific WGA-AF488 staining of hyphal walls (λexc494 nm, λem515) **(B)** Detection of *Si*sRNAs in roots at 3-, 7- and 14 dpi using multiplexed stem-loop PCR. Agarose gel analysis of *Si*sRNA detected bands of the expected size of 62 bp. Plant *At*miR159a was used as a positive control for a plant-expressed sRNA.

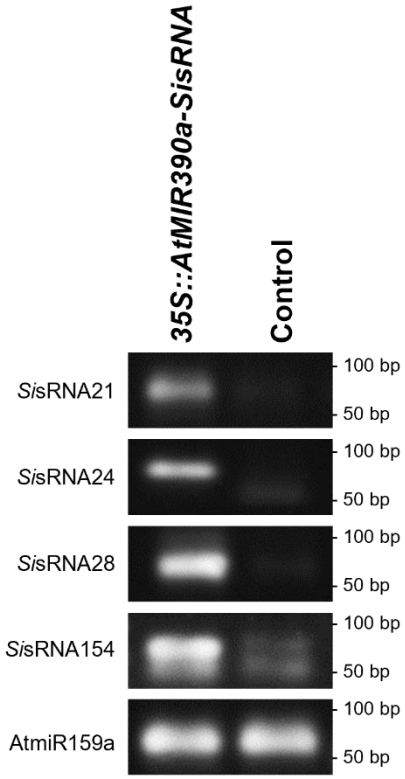

Figure 7. Duplexed stem-loop PCR confirming expression of *Si*sRNAs in Arabidopsis protoplasts. Agarose gel analysis of stem-loop PCR confirmed the detection of all four expressed *Si*sRNA in transformed protoplasts 24 hptr, but not in control protoplasts. Plant *At*miR159a was used as a positive control.

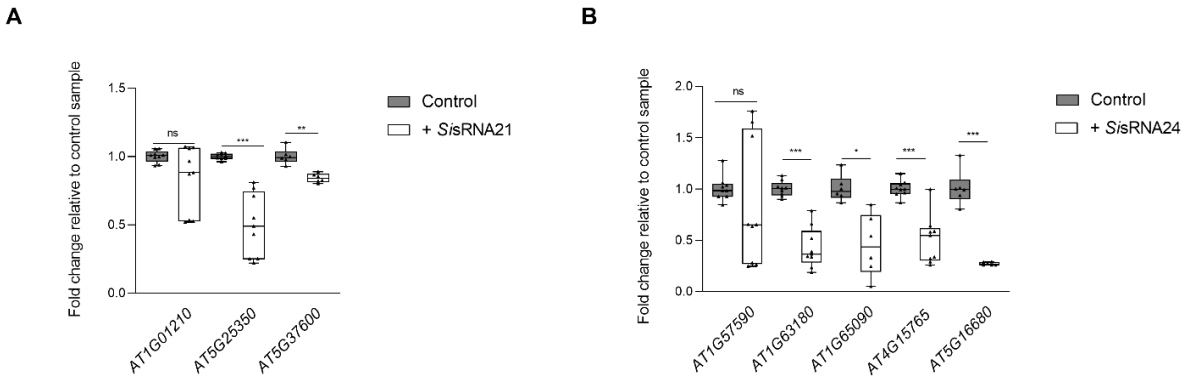

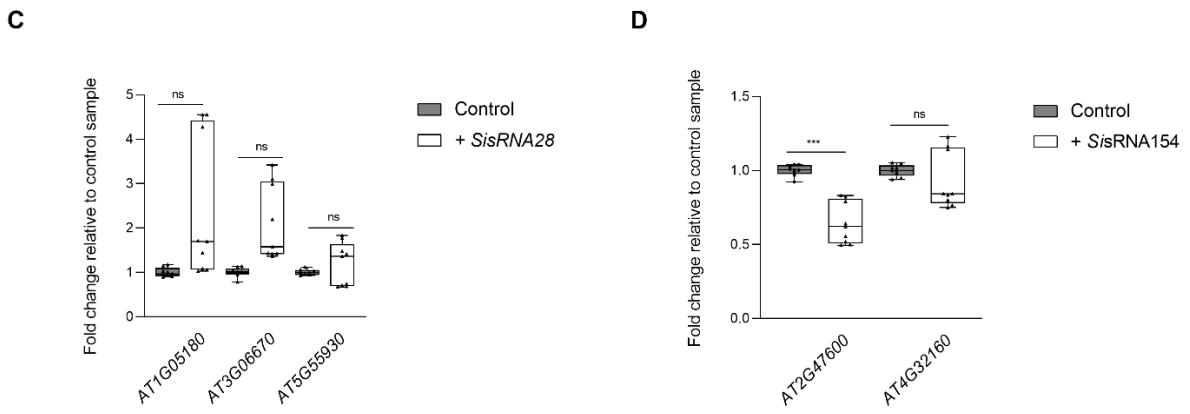

Figure 8. qPCR analysis of target gene silencing in Arabidopsis protoplasts 24 hptr with *Si*sRNAs vs. control (protoplast without *Si*sRNA construct). The mRNA transcript levels in transformed protoplasts (+) expressing **(A)** *Si*sRNA21, **(B)** *Si*sRNA24, **(C)** *Si*sRNA28 and **(D)** *Si*sRNA154 normalized against housekeeping gene *Ubiquitin* (*AT3G62250*) are displayed as fold change relative to control protoplasts. Data are the average of two to three biological replicates ± standard deviation. Asterisks indicate difference at $p \leq 0.05$(*), $p \leq 0.01$ (**) and $p \leq 0.001$ (***) according to Student's t-test. ns= not significant.

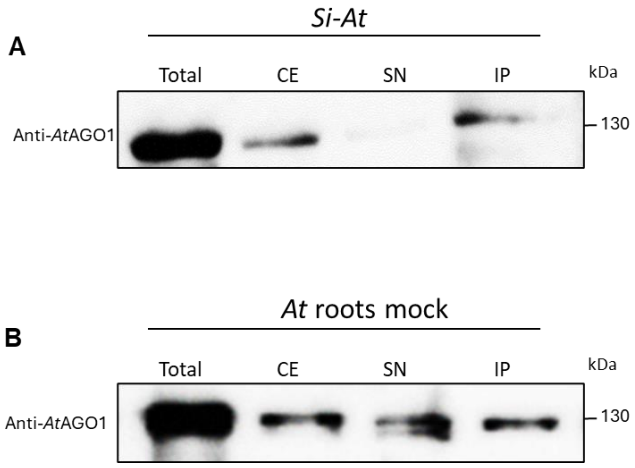

Figure 9. Quality control of AGO1 co-immunoprecipitation by western blot. Four sample fractions of the AGO1 co-IP experiment were analyzed: total protein before centrifugation and debris removal, crude extract (CE) after centrifugation and debris removal, supernatant (SN) after incubation with anti-*At*AGO1 and agarose beads, and IP fraction (resuspended IP pellet). These four fractions were analyzed in **(A)** *Si*-colonized root samples and **(B)** in *At* mock-treated roots. Both figures show the detection of *At*AGO1 using anti-*At*AGO1-specific antibody at the expected size of ~ 130 kDa. Note that AGO1 signals were stronger in IP fractions than in SN. The broad-range pre-stained protein marker was used as a protein-size marker.

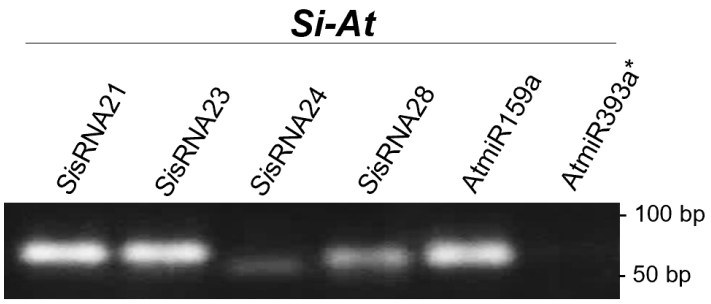

Figure 10: *Si*sRNAs co-immunoprecipitated with *At*AGO1 in *Si*-colonized Arabidopsis roots. Stem-loop PCR analysed in agarose gel confirms the presence of *Si*sRNA21, *Si*sRNA23, *Si*sRNA24, *Si*sRNA28, as well as AGO1 bound *At*miR159a but not AGO2 bound *At*miR393a* in *At*AGO1-co-IP samples from *Si*-colonized *At* roots.